SATIF-15:
15th Workshop on Shielding aspects of Accelerators, Targets, and Irradiation Facilities

Facility for Rare Isotope Beams (FRIB) at Michigan State University
East Lansing, Michigan USA
20-23 September 2022.

Session 6: Shielding & Dosimetry

Table of contents

1. Radiological assessment for the renovation of the CERN East Area primary area and secondary beam lines

Arnaud Devienne[1*], Robert Froeschl[1], Jean-François Gruber[1]
[1]CERN, European Organization for Nuclear Research, 1211 Geneva 23, Switzerland
[*]arnaud.devienne@cern.ch

The East Area renovation project aimed at completing by the end of Long Shutdown 2, the consolidation and renovation of the CERN East Area, served by the Proton Synchrotron accelerator since more than 55 years. In particular, the Primary Area and the secondary beam lines of the East Area have been completely redesigned within a renovation project, in which ambitious technical specifications applied to an existing old facility have highlighted some safety challenges to face.

The East Area receives a primary proton beam from the Proton Synchrotron at a beam momentum of 24 GeV/c and an average beam intensity of 6.6e10 protons per seconds. The primary beam can then impact on dedicated targets located in the Primary Area, to produce secondary beams for test beam lines T9, T10 and T11 allowing them to realize a wide range of experiments from 15 GeV/c down to low beam momenta. The primary beam from the Proton Synchrotron can also be directly transported through the T8 beam line to the IRRAD and CHARM facilities located inside the East Area.

This study details the challenges behind the radiological assessment of the new layout of the East Area after its renovation, starting with the preparation and dismantling of the old installation. Then, the focus is brought on the design of the shielding structure and the drivers of the radiological assessment performed, showing the demanding constrains and the resulting compromises made to achieve prompt ambient dose equivalent rate levels compatible with the CERN radiological area classification. The design of the renovated East Area has also been optimized with respect to the residual radiation levels. In particular, the number of beam line elements and size of the Target Area have been minimized. A Mixed Area, physically separated by a thick beam dump from the Target Area, has been created containing most of the beam line elements of the secondary lines thereby reducing the dose received during interventions on beam line elements. Besides, a ventilation system for the Primary Area has been designed to provide dynamic confinement with a design objective for the air tightness of 1 air volume of the facilities per hour, limiting the committed effective dose due to inhalation during accesses even after short cool-down time. Finally, the study details the results of the commissioning phase, the measurements performed during this first year of operation, and the continuous beam optimization to minimize both the prompt and residual radiation while fulfilling the beam specifications for the users.

The locations of the radiation area monitors have also been redesigned according to the new layout of the East Area, to verify the compliance of the area classification limits. The measurement data from the radiation monitor network coupled with the shielding calculations performed with FLUKA for the different scenarios, has proven to provide useful feedback during the commissioning phase and in normal operation.

1.1 Introduction

The East Area renovation project (2016-2021) aimed at completing by the end of Long Shutdown 2 (LS2) the consolidation and renovation of the CERN East Area (EA), served by the Proton

Synchrotron accelerator (PS) since more than 55 years (Bernhard et al., 2021). It includes a re-design of the production target complex and the secondary beam lines T9, T10 and T11. The main motivations of the project are to have energy efficient magnets for energy savings and reliability, positive production angles for the secondary beams to exclude accidental scenarios, a dedicated main dump for prompt radiation, to improve the accessibility in areas of higher activation for residual radiation and a ventilation system for the primary areas for air activation. The other existing facilities of the East Area, named IRRAD and CHARM (Froeschl et al., 2015; Froeschl et al., 2018), have not been modified from a radiological point of view during the project.

The East Area is housed in building 157 and receives a primary proton beam from the CERN PS via the F61 transfer line with a maximum beam momentum of 24 GeV/c, up to 5e11 protons per pulse and an average design beam intensity of 6.6e10 protons per second. This study summarizes the radiological assessment made for the renovation of the East Area and its secondary beamlines. The radiation protection studies have been performed using the Monte Carlo code FLUKA hosted by CERN v4-2.2 (Ahdida et al., 2022; Battistoni et al., 2015). The results presented in this study are then compared with measurements performed during commissioning and along the 1st year of operation after the East Area renovation.

1.2 Facility description

The East Area renovation project implies a new design of several elements, particularly on the shielding configuration. The general layout of the East Area before LS2 is shown in Figure 1.1 and can be compared with the general layout after the completion of the East Area renovation during LS2, shown in Figure 1.2, including the new locations of the radiation monitoring system. After the renovation, the East Area contains the following areas interlocked by the access system:

- *Primary Area* further divided in 3 sectors: the *Target Area* (containing T9 and T10 targets, T11 Beam Stopper Dump and T8a beam line elements), the *Mixed Area* (containing T9, T10 and T11 beam lines elements together with T9 and T10 Beam Stopper Dumps) and the *T8b-T8c Areas* (containing the T8 Beam Stopper shielding together with T8b and T8c beam line elements upstream of IRRAD and CHARM).
- *T9-10 Zone*: downstream the Mixed Area, it contains T9 and T10 beam line elements.
- *T9 Experimental Area*: downstream the T9-10 Zone, it contains T9 beam line detectors.
- *T10 Experimental Area*: downstream the T9-10 Zone, it contains T10 beam line detectors.
- *T11 Experimental Area*: downstream the Mixed Area, it contains T11 beam line detectors and the CLOUD experiment (Cosmic Leaving Outdoor Droplets).
- *IRRAD&CHARM* facilities: located downstream T8b-T8c Areas in the south part of the East Area Hall, they have a dedicated interlocked area composed of 3 sectors. The facilities have not been modified from a radiological point of view during LS2.

In addition, the *PS to EA extraction area* is located upstream of the East Area in building 352 and formally belongs to the PS access system. It contains the F61 extraction beam line, able to extract the beam from the PS to the East Target Area, or alternatively to send it to the East Dump located downstream of the PS to EA extraction area. The schematic layout of the East Area beam lines is shown in detail in section 1.4 together with the drivers considered for the radiological assessment.

Figure 1.1. East Area layout before LS2

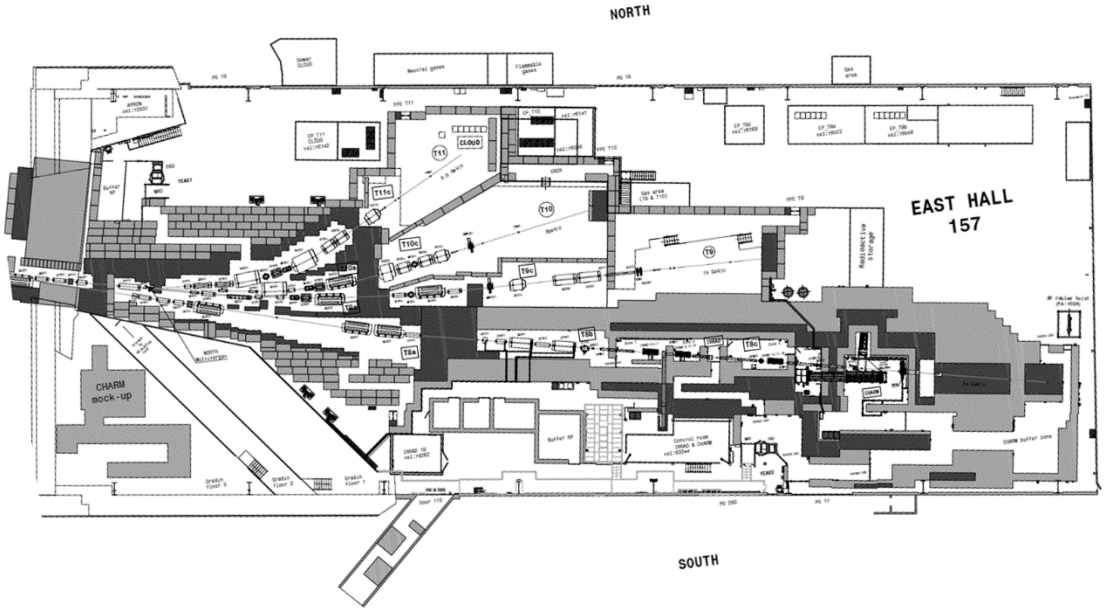

Source: CERN (2022).

Figure 1.2. East Area layout after LS2 (including the new radiation monitoring system)

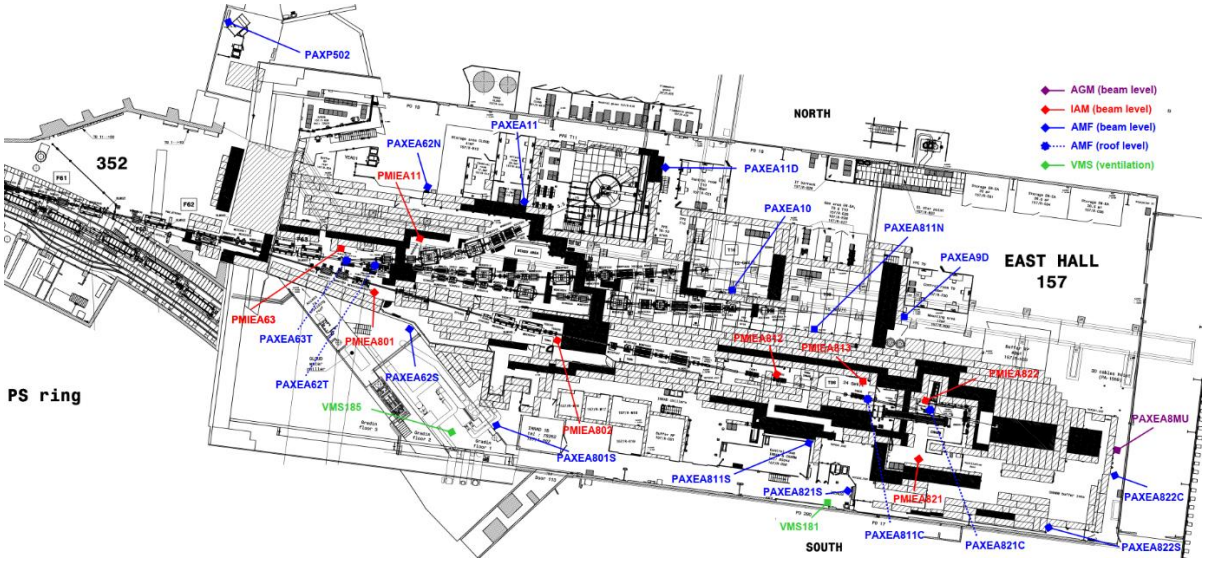

Source: CERN (2022).

1.3 Dismantling

To carefully plan the radiological aspects of the dismantling of the former East Area primary area and secondary beamlines, two dossiers of intervention in radiation areas have been created (one for the Transfer line and one for the Primary Area) to optimize the doses received during the dismantling following the ALARA principle (As Low As Reasonably Achievable). Each dossier has then been divided in subtasks for a close dosimetry follow-up along the dismantling period. No further level of detailed was added to keep the estimates operationally manageable.

The dismantling of the East Area has been classified internally at CERN as an ALARA 3 intervention, after estimating that the collective dose would be above the threshold of 5 man.mSv. This means that the intervention and its specific optimization measures have been presented and approved in a dedicated ALARA committee.

At the end of the dismantling, the measured collective dose has been 4.4 man.mSv (for an estimated of 6.1 man.mSv), and the maximum individual dose 0.4 mSv (for an estimated of 0.6 mSv). However, although the values resulting values per dossier were slightly below the estimated values, there have been some subtasks ending above (e.g. difficulties found during the dismantling tasks) while other finally appeared lower than the estimations (e.g. quicker time of execution and more optimized working conditions).

The evolution of the collective dose over time by dossier can be observed on Figure 1.3. Two specific increases of the collective dose occurred in June and July 2019 during the removal of the target and during the removal of the TCX collimator, being by design the most activated elements of the installation.

Finally, the volume of radioactive waste produced was about 40 m³ and most of the radioactive shielding blocks have been re-used in the new shielding design.

Figure 1.3. Cumulative collective dose over time by dossier during the dismantling

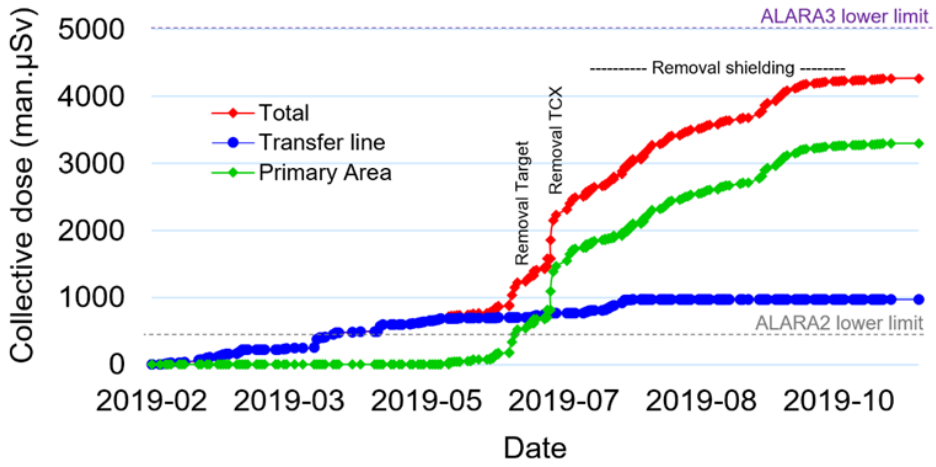

Source: CERN (2022).

1.4 Design parameters

The scenarios and drivers for the shielding design consider a beam loss in the PS, a commissioning beam sent to East Dump, an accidental beam loss to T8, a standard primary beam to T9 and T10/11 targets, and a standard secondary beam to the experimental area dumps. A schematic view of the beam line layout, including the areas concerned by the scenarios and drivers is shown on Figure 1.4. The maximum momentum of the primary proton beam destinated to the East Dump, the T8 beam line or to the T9 and T10/11 targets is 24 GeV/c, while for the secondary beam the maximum particle momenta considered are 15 GeV/c, 12 GeV/c and 3.5 GeV/c respectively for T9, T10 and T11 secondary beam lines.

The design criteria for the radiological area classification are summarized in Table 1.1. In particular, the aim is to keep the East Hall withing the limits of *Supervised Radiation Area* for prompt radiation (with permanent workplace for the control rooms and low occupancy for the hall and experimental areas when accessible), while some technical zones will be classified as *Simple Control Radiation Area* (e.g. IRRAD lateral, buffer zones and T9-10 Zone when accessible).

The simulations, performed with FLUKA hosted by CERN v4-2.2, use the PRECISIO settings for the DEFAULT card. The hadrons transport thresholds are set to 10 MeV, except neutrons which are followed down to thermal energy of 1e-14 GeV. The electromagnetic shower has been turned OFF with EMF card, except during residual transport. Finally, coalescence and evaporation with heavy fragment has been enabled. Biasing techniques and CPU time usage were optimized to ensure scorings with statistical errors at least below 20% in all the areas of interest.

The monitoring system is composed for prompt radiation of 16 Area Mixed Field IG5-H20 monitors (AMF) to measure the neutron field outside the shielding enclosures, and 1 Area Gamma-Muon IG5-A20 monitor (AGM) to measure the muon component. For residual radiation, 8 Induced Activity Monitors (IAM) are available to measure photons generated by the activated component in the Primary Area and in IRRAD&CHARM. Finally, the air releases to the environment are monitored by 2 Ventilation Monitoring Stations (VMS). The layout of the monitoring system after the East Area renovation was previously shown on Figure 1.2.

Figure 1.4. Schematic view of the beam lines with drivers and scenarios for the assessment

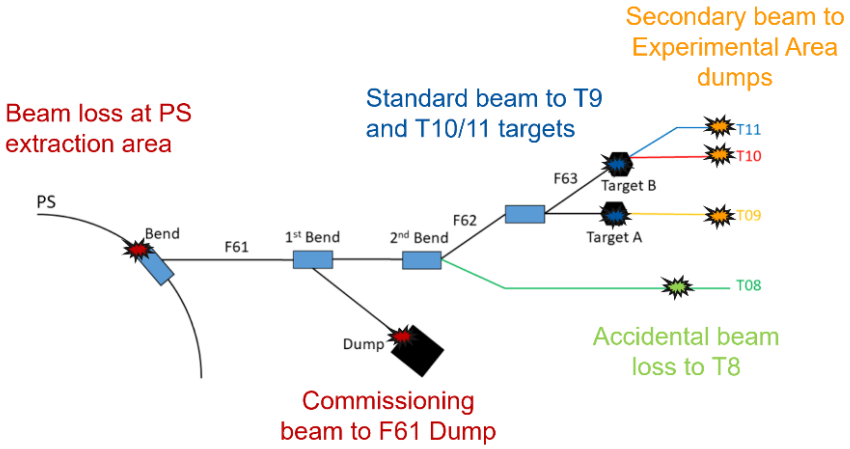

Source: CERN (2022).

Table 1.1. CERN radiological area classification

	Area	Annual dose limit (year)	Ambient dose equivalent rate	
			permanent occupancy	low occupancy
	Non-designated	1 mSv	0.5 µSv/h	2.5 µSv/h
Radiation Area	Supervised	6 mSv	3 µSv/h	15 µSv/h
Radiation Area	Simple Controlled	20 mSv	10 µSv/h	50 µSv/h
Radiation Area	Limited Stay	20 mSv	-	2 mSv/h
Radiation Area	High Radiation	20 mSv	-	100 mSv/h
Radiation Area	Prohibited	20 mSv	-	> 100 mSv/h
Controlled Area				

Source: CERN (2022).

1.5 Results

The radiological assessment for the renovation of the East Area cover prompt radiation, residual radiation, air activation, and releases to the environment. The simulations performed consider a series of scenarios by area summarized in Table 1.2. For each scenario the results of the simulations are detailed and then compared whenever possible with measurements performed during the commissioning and the first year of operation.

Table 1.2. Scenarios considered for the radiological assessment and commissioning

#	Description	Beam Momentum	Beam intensity	Target	Comments
1	Continuous beam loss in PS	24 GeV/c	5.0e9 proton/s	Cu target (50 cm)	Estimated intensity
2	Commissioning beam to F61 Dump	24 GeV/c	2.3e9 proton/s	Cast iron dump (240 cm)	Estimated intensity
3	Beam toward T9 target	24 GeV/c	3.3e10 proton/s	Al (20 cm)	Beam stoppers T9, T10 and T11 all closed
4	Beam toward T10/11 target	24 GeV/c	3.3e10 proton/s	Al (20 cm)	Beam stoppers T9, T10 and T11 all closed
5	Full beam loss toward T8	24 GeV/c	6.6e10 proton/s	Cu (50 cm)	Accidental scenario
6	Secondary beam on T9 Dump	15 GeV/c	3.3e5 pion/s	Cast iron dump (240 cm) + Concrete (80 cm)	Intensity generally lower by a factor 10
7	Secondary beam on T10 Dump	12 GeV/c	3.3e5 pion/s	Cast iron dump (160 cm) + Concrete (80 cm)	Intensity generally lower by a factor 10-
8	Secondary beam on T11 Dump	3.5 GeV/c	3.3e5 pion/s	Cast iron dump (160 cm)	Intensity generally lower by a factor 10

Source: CERN (2022).

1.5.1 Prompt radiation at the PS to EA extraction area

The assessment of the areas located between the PS and the East Area highlights the challenges of intermediate stages during the design and the commissioning phases. Indeed, the Target Area (not accessible when beam extracted to the East Area is ON, and dominated by residual radiation when the beam is OFF) was frequently accessed during the renovation to install beamlines elements. At the end of LS2 the beam was already circulating in the PS (with the extraction to the East Area interlocked) so the possible losses in the PS in vicinity of the extraction area (scenario #1 from Table 1.2) were assessed with FLUKA simulations (see Figure 1.5, left plot) and monitored during the commissioning of the PS-to-EA shielding interface. The active monitoring during PS operation from 01/03/2021 to 01/05/2021 shows dose rates measurements in agreement with expected values, with background reading in operation at the B.352 PS access, at the Target and the East Hall.

Later, a dedicated commissioning test on the East Dump (scenario #2 from Table 1.2) was performed on 14/03/2022. The goal was to compare the ambient dose equivalent rate values at the B.352 PS access location (PAXP502) between the simulations and the measurements. The test was done at several extraction intensity steps by changing the value of protons per pulse. The measurements on Figure 1.6 first show that dose rate scales linearly with the beam intensity, secondly that a value of 0.17 µSv/h (±0.01) is measured when no beam is extracted corresponding to the monitor background accounting the contribution of beams circulating in the PS during the test, and finally that the limit of 2.5 µSv/h (±0.14) is reached for an average beam intensity of 7.0e9 proton/s. The value can be compared with the dose map of the simulations, assuming a perfect extraction and obtaining an intensity of 2.3e9 proton/s on the East Dump to reach a comparable net contribution of 2.33 µSv/h (±0.02) at the PAXP502 location (see Figure 1.5, right plot).

Figure 1.5. Prompt radiation at PS to EA extraction area (scenario #1 and #2 from Table 1.2)

Left: Continuous beam loss in PS (scenario #1 from Table 1.2)
Right: Commissioning beam to F61 Dump (scenario #2 from Table 1.2)

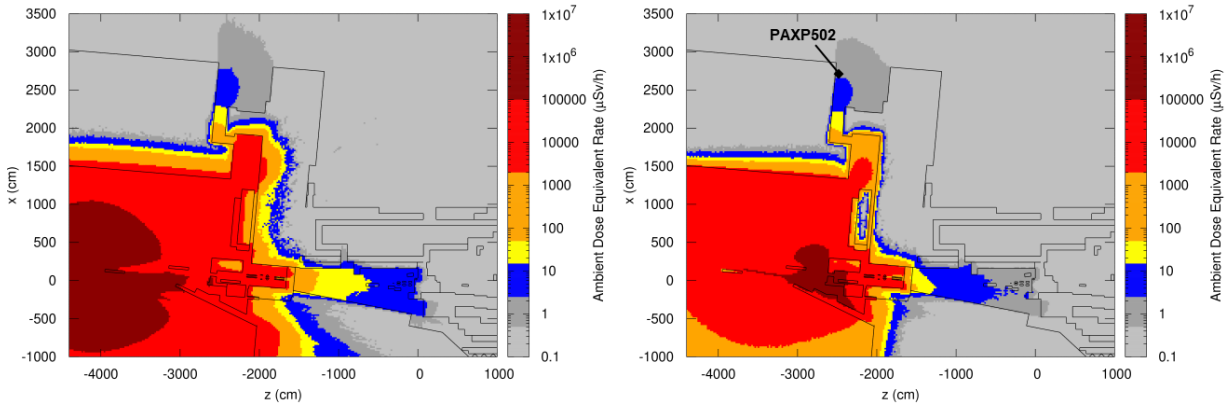

Note: Colour scale in agreement with radiological area classification (see Table 1.1). Source: CERN (2022).

Figure 1.6. Average dose rate measured at the B.352 PS access location (radiation monitor PAXP502) as a function of the average beam intensity to the East Dump destination.

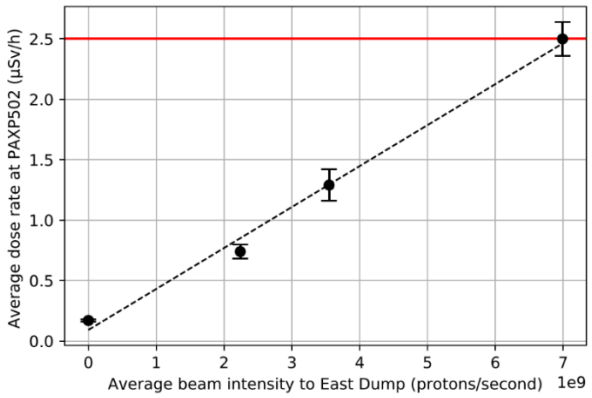

Note: The limit for non-designated area low occupancy is marked as red line. Source: CERN (2022).

1.5.2 Prompt radiation at the Primary Area

The core of this radiological assessment concerns the shielding of the Primary Area. The areas of interest and the challenges faced during the design of the Primary Area have been:

- the *Ventilation platform* (laterally of the Target Area) due to the primary beam directly impacting the targets at that level. To shield the area, shielding columns have been placed laterally to the target and additional blocks on the floor of the Ventilation platform.
- the *Primary Area access maze entrance* (north part of the East Hall), due to the secondaries produced in the Target Area. The length of the maze and the shielding geometry have led to an optimized design, shielding efficiently both the component coming directly from the targets and the produced neutrons streaming through the openings.
- the *T9/10 Zone* (downstream the Primary Area), due to the space and mechanical constrains found in the design to shield efficiently the muon component originated in the Primary Area dump and the neutron component contributing to the total ambient dose equivalent in the area. Indeed, most of the muons produced go between the magnets and their support, making the design of efficient local shielding challenging.

- The *Roof* (above the Target Area), due to the significant shielding thickness required (4m of concrete with a first layer of 80 cm of cast iron), and the building ground load constraints associated. Optimization of its design has been done with this regard, by removing blocks from the design whenever the results from the simulations made it acceptable.
- The T11 Control Room (laterally to the Mixed Area), due to its location regarding the Primary Area dump and its area classification of Supervised Radiation Area (permanent workplace). Reinforcement of the Primary Area shielding wall with cast iron and local shielding was added in the design phase to limit the dose in this area.

The results of the simulations for the operational scenario of the Primary Area (sum of scenarios #3 and #4 from Table 1.2) are shown in Figure 1.7, showing the attenuation of the radiation through the massive shielding enclosure.

Figure 1.7. Prompt Ambient Dose Equivalent rates around the Primary Area (sum of scenarios #3 and #4 from Table 1.2)

Top: horizontal cut at primary beam level (100 cm < Y < 140 cm)
Bottom: vertical cut at primary beam axis (-20 cm < X < 20 cm)

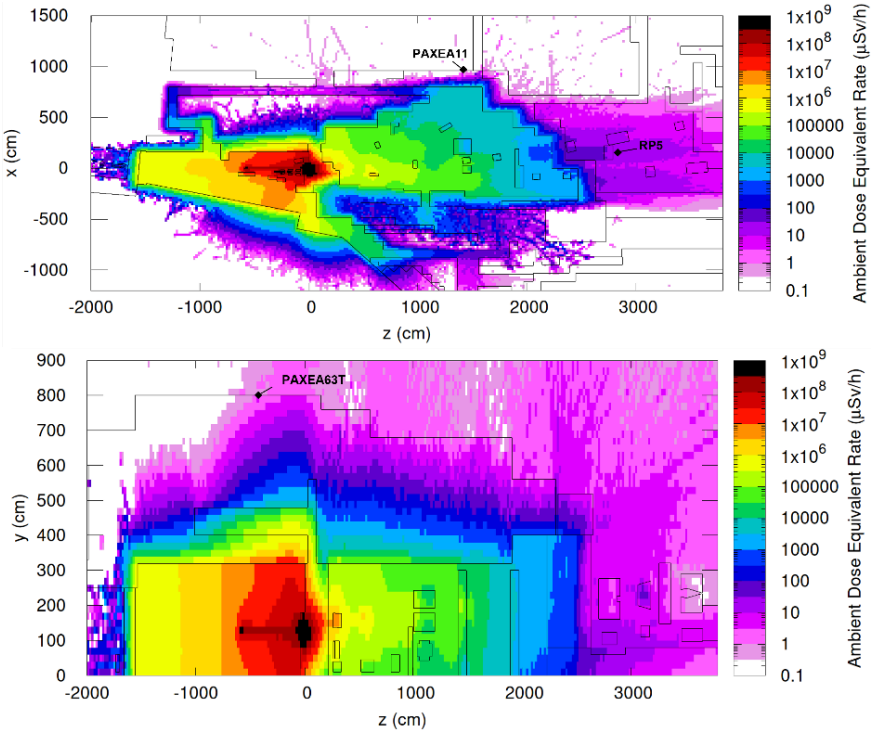

Source: CERN (2022).

Then, measurements have been performed on 03/09/2021 and 04/09/2021, using and average intensity of 1.12e10 proton/s sent exclusively on T9 target during 1h, followed by a period with an average intensity of 1.72e10 proton/s sent exclusively on T10 target during 1h. When adding both contributions and scaling the measurements to the design intensities from Table 1.2 (in order to be compared with Figure 1.7), the following net values measured by the radiation monitors are obtained: 2.5 µSv/h (± 0.13) on the Ventilation platform (PAXEA62S monitor), 0.11 µSv/h (± 0.08) on the Roof (PAXEA63T), 17 µSv/h (± 0.64) in the T9/10 Zone (RP5 mobile monitor), and 0.24 µSv/h (± 0.08) at the T11 Control Room (PAXEA11). The results for all locations are compatible with the radiation area classification, with measured values below the simulated values partly due to a conservative approach of the calculations such as for the use of lower densities for shielding materials in the FLUKA geometry (2.2 g/cm^3 for concrete and 7.2 g/cm^3 for cast iron).

Finally, the skyshine radiation calculations performed with FLUKA resulted in an annual ambient dose equivalent of 0.65 µSv for persons of the reference group for members of the public located at a radius of 300 m from the East Area, using a nominal annual beam intensity of 3.3e17 proton/year. The value is below the objective of 1.0 µSv for the East Area (10 µSv for all CERN facilities). No discrimination by CERN installation can be obtained on the annual measurements, however the actual contribution of the East Area is expected to be lower than the simulated value, considering the lower dose rates measured on the Primary Area roof comparing to the simulations.

1.5.3 Prompt radiation at the Experimental Areas

The shielding design of the Experimental Areas aims at protecting people in accessible locations when the beam lines are in operation using secondary beams (i.e. in Control Rooms T9, T10 and T11, and in East Area Hall), but also against secondary particles originated upstream and propagating in the forward direction downstream to the Experimental Areas. The simulations of the secondary beam scenarios in the T9, T10 and T11 experimental areas are shown in Figure 1.8. Measurements performed during the commissioning and operation of the experimental areas are compatible with the radiological area classification. On 07/10/2021 during the commissioning of T9 experimental area and scaling the measurements to the design intensities intensity from Table 1.2, a net contribution of 0.04 µSv/h (± 0.01) has been measured at a location of interest downstream T9 dump area (PAXEA9D monitor), while values at the experimental area access maze entrance (RP6 mobile monitor) were found to be negligible. All the measurements in the experimental areas during the commissioning and the first year of operation are compatible with the *Supervised Radiation Area* classification of the East Hall.

Figure 1.8. Prompt radiation around Experimental Areas (scenarios #6, #7 and #8 from Table 1.2)

Left: T9 secondary beam (scenarios #6 from Table 1.2). Centre: T10 secondary beam (scenarios #7 from Table 1.2). Right: T11 secondary beam (scenarios #8 from Table 1.2)

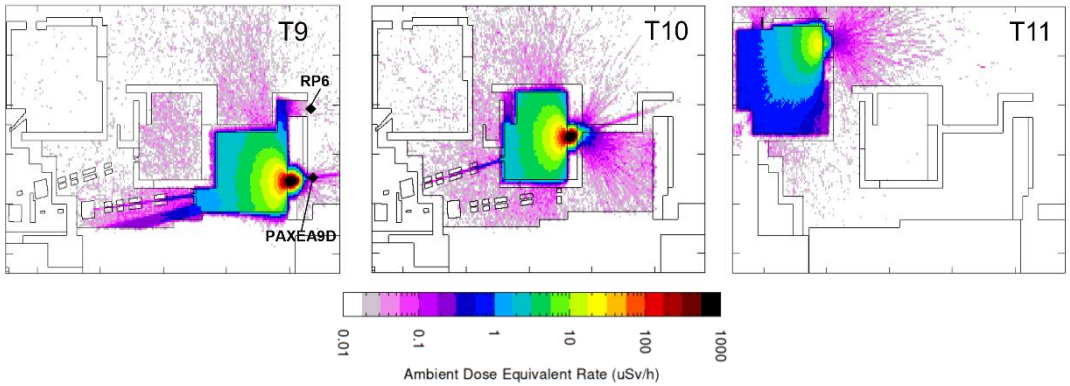

Source: CERN (2022).

1.5.4 Residual radiation

The design of the facilities has been optimized with respect to the residual radiation levels. The residual ambient dose equivalent rates in the Target Area remains to levels well below 100 mSv/h after 1 hour of cool-down at the worst locations, which can be optimized with the use of movable shielding. The targets or any other highly activated element can also be removed in case of interventions after short cool-down time via plug-in systems. The simulations have been performed scoring residual ambient dose equivalent rate after 20 years of operation at design intensity, for different cool down times from 1 second up to 10 years. Figure 1.9 shows the results of the simulations scoring residual ambient dose equivalent after 1 hour, 1 day and 10 years of cool-

down. The radiation surveys performed in this area in 2021 and 2022 (after less than a year of operation) preliminary confirmed that the residual radiation is well contained in the Target Area, fulfilling the design criteria of the Primary Area, and giving the possibility of optimized interventions in the Mixed Area even after short cool down times (<1 day).

Figure 1.9. Residual dose rate in the Primary Area after 20 years of operation at design intensity

Cool-down times: 1 hour (top), 1 day (middle) and 10 years (bottom)

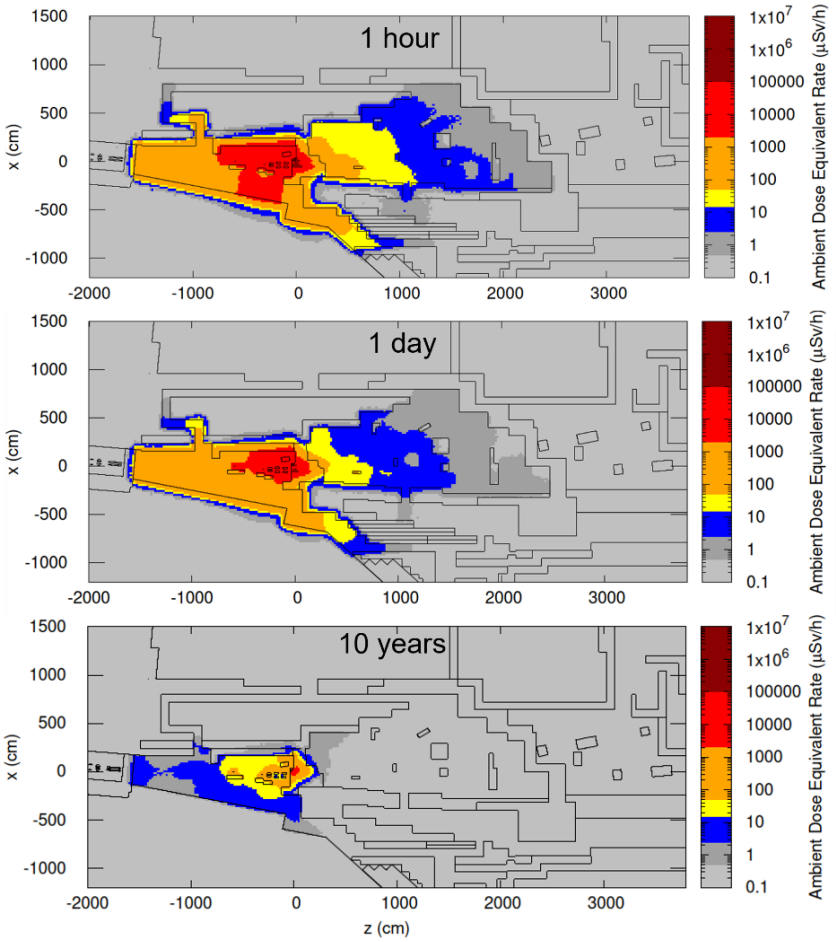

Note: Colour scale in agreement with radiological area classification (see Table 1.1). Source: CERN (2022).

1.5.5 Air activation and releases to the environment

A ventilation system for the Primary Area has been designed to provide dynamic confinement with a design objective for the air tightness of 1 air volume of the facilities per hour. Even without the mandatory flush before access, the committed effective dose due to inhalation for a 1-hour access is expected to be approximately 0.3 µSv, i.e. well below the design objective of 1 µSv. The following methodology (Froeschl et al., 2018) has been applied to compute the radionuclide concentrations, the annual release to the environment and the resulting annual effective dose to members of the public, summarized in Table 1.3:

- The track-length spectra for protons, neutron and charged pions have been scored in the air volumes with FLUKA and then folded with air activation cross-sections to obtain the radionuclide production yields.

- The radionuclide concentrations in the facility and the release term to the environment have been calculated from the radionuclide production yields considering the time evolution, the characteristics of the ventilation circuit and an annual intensity of 1e18 proton/year sent to the East Area facilities.
- The radionuclide concentrations in the facility after beam stop have been converted to the committed effective dose due to inhalation without flush for a 1-hour access, by application of exposure-to-dose conversion coefficients for inhalation and considering the decay time.
- The release term has been converted to the effective dose to members of the public by application of release to effective dose conversion coefficients, computed based on models for environment impacts of CERN facilities (Vojtyla, 2015).

Table 1.3 Radiological impact of air activation in the Target Area

Radionuclide	Production yield	Total Activity after beam stop	Committed effective dose due to inhalation without flush* for 1 hour access	Release environment	Effective dose to members of public
	nucl./primary	Bq	μSv	TBq/y	μSv/y
H-3	2.32E-03	9.81E+02	1.61E-04	5.18E-06	2.10E-07
Be-7	5.55E-04	1.98E+04	3.65E-03	1.05E-04	1.46E-03
Be-10	4.33E-04	1.41E-03	1.07E-07	7.46E-12	7.46E-10
C-11	8.26E-04	3.66E+07	7.20E-02	1.93E-01	1.02E-02
C-14	8.84E-01	8.06E+02	1.87E-03	4.25E-06	2.48E-05
N-13	1.24E-03	6.60E+07	2.47E-02	3.49E-01	1.34E-02
O-14	7.02E-05	4.51E+06	3.83E-11	2.38E-02	5.47E-04
O-15	8.64E-04	5.44E+07	1.26E-06	2.87E-01	3.82E-03
O-19	9.51E-08	6.21E+03	8.74E-27	3.28E-05	1.51E-07
F-18	1.70E-06	3.08E+04	7.90E-03	1.63E-04	9.42E-05
Ne-23	2.07E-07	1.35E+04	0.00E+00	7.13E-05	3.79E-08
Ne-24	4.81E-08	2.94E+03	0.00E+00	1.55E-05	1.71E-07
Na-22	5.63E-07	1.13E+00	9.03E-06	5.96E-09	3.49E-05
Na-24	8.31E-07	2.42E+03	4.90E-03	1.28E-05	1.69E-04
Na-25	3.47E-07	2.24E+04	0.00E+00	1.18E-04	3.32E-07
Mg-27	4.34E-07	2.33E+04	0.00E+00	1.23E-04	9.90E-05
Mg-28	1.40E-07	2.96E+02	1.95E-03	1.57E-06	2.10E-05
Al-26	7.86E-07	5.73E-06	3.21E-10	3.02E-14	2.10E-09
Al-28	1.93E-06	1.21E+05	0.00E+00	6.38E-04	4.69E-04
Al-29	8.11E-07	4.62E+04	0.00E+00	2.44E-04	1.65E-05
Si-31	1.20E-06	1.66E+04	5.61E-03	8.74E-05	2.02E-05
Si-32	6.76E-07	7.84E-03	1.72E-06	4.14E-11	8.69E-09
P-30	6.07E-07	3.78E+04	0.00E+00	2.00E-04	7.90E-06
P-32	7.43E-06	9.89E+02	1.15E-02	5.22E-06	1.82E-04
P-33	5.68E-06	4.26E+02	2.21E-03	2.25E-06	1.26E-05
P-35	6.42E-07	4.16E+04	0.00E+00	2.20E-04	1.33E-04
S-35	7.46E-06	1.63E+02	7.15E-04	8.58E-07	4.25E-06
S-37	2.46E-06	1.45E+05	0.00E+00	7.64E-04	7.12E-05
S-38	1.30E-06	1.67E+04	0.00E+00	8.81E-05	1.66E-04
Cl-34	2.90E-07	1.08E+04	0.00E+00	5.71E-05	0.00E+00
Cl-36	1.76E-05	3.05E-04	6.23E-09	1.61E-12	7.52E-09
Cl-38	1.32E-05	4.60E+05	4.62E-02	2.43E-03	8.62E-04
Cl-39	2.38E-05	6.72E+05	9.90E-02	3.55E-03	1.59E-03
Cl-40	3.34E-06	2.13E+05	0.00E+00	1.13E-03	3.95E-05
Ar-37	6.18E-05	3.36E+03	0.00E+00	1.77E-05	1.52E-12
Ar-39	9.64E-05	1.87E+00	0.00E+00	9.87E-09	3.22E-12
Ar-41	1.87E-03	3.39E+07	0.00E+00	1.79E-01	1.39E-02
K-38	2.40E-07	1.34E+04	0.00E+00	7.07E-05	2.34E-05
K-40	1.02E-06	4.16E-09	4.99E-14	2.20E-17	2.31E-13
Total			0.28	1.04	0.047

*These are hypothetical values used only in the assessment. A flush is always performed before access and, with a flush volume of 3 total air volumes, results in a reduction by a factor of 20.

Source: CERN (2022).

1.6 Summary and conclusions

The renovation of the Primary Area and secondary beam lines of the CERN East Area has been performed during the period 2016-2021. The shielding has been designed so that the prompt ambient dose equivalent rate levels for the average design beam intensity of 6.6e10 protons per second are compatible with the CERN radiological area classification. This study details the challenges behind the radiological assessment of the new layout of the East Area after its renovation, starting with the preparation and dismantling of the former facility. The design of the

shielding structure has highlighted the demanding constrains and the resulting compromises made to achieve radiation levels compatible with the radiological area classification. The design has also been optimized with respect to the residual radiation levels. In particular, the size of the Target Area and its number of elements have been minimized. A Mixed Area containing most of the secondary beam line elements has been constructed separated physically from the Target Area by a thick beam dump to reduce the doses received during interventions. In addition, a ventilation system for the Primary Area has been designed to provide dynamic confinement, limiting the committed effective dose due to inhalation during accesses even after short cool-down time.

Finally, the radiation protection study compares the results of FLUKA simulations with the measurements performed during the commissioning and the first year of operation. The results are compatible with the radiological area classification of the East Area foreseen during the design, with a good agreement with the simulations, generally better than a factor of 2 when comparing ambient dose equivalent rates. The locations of the radiation monitors have also been redesigned according to the new layout of the East Area, to verify the compliance with the area classification limits. Besides, the measurements from the radiation monitor network coupled with the shielding calculations performed with FLUKA for the different scenarios, has proven to provide useful feedback during the commissioning phase and in normal operation. In summary, it has been demonstrated that the design of the East Area Primary Area and secondary beam lines facilities fulfils the CERN radiation protection requirements in an optimized fashion and can safely operate at the design intensity from a radiological point of view.

1.7 List of references

Bernhard J. et al. (2021), “CERN Proton Synchrotron East Area Facility Upgrades and renovation during Long Shutdown 2”. Yellow report CERN–2021–004.

Froeschl R. et al. (2015), “The CERN High Energy Accelerator Mixed Field (CHARM) facility in the CERN PS East Experimental Area”, Proceedings of SATIF 12, NEA/NSC/R.

Ahdida C. et al. (2022), "New Capabilities of the FLUKA Multi-Purpose Code", Frontiers in Physics 9, 788253

Battistoni G. et al. (2015), "Overview of the FLUKA code", Annals of Nuclear Energy 82, 10-18.

Froeschl R. et al. (2018), “Radiation Protection Aspects of the Commissioning and Operation of the CERN High Energy Accelerator Mixed Field (CHARM) facility in the CERN East Experimental Area”, Proceedings of SATIF 13 NEA/NSC/R.

Vojtyla P. (2005), “Models for environmental impact assessments of releases of radioactive substances from CERN facilities”. Technical Report CERN–SC–2005–005–IE, EDMS 607969.

1.8 List of abbreviations and acronyms

ALARA	As Low As Reasonably Achievable
CERN	Conseil Européen pour la Recherche Nucléaire
CHARM	Cern High energy AcceleRator Mixed-field
CLOUD	Cosmic Leaving Outdoor Droplets
EA	East Area
IRRAD	IRRADiation proton facility
LS2	Long Shutdown 2
PS	Proton Synchrotron

2. Radiation protection assessment of the AMBER Drell-Yan program

Claudia Ahdida[1*], Arnaud Devienne[1], Vincent Andrieux[2], Dipanwita Banerjee[1], Johannes Bernhard[1], Serhii Cholak[3], Carlos Davide Da Rocha Azevedo[4], Oleg Denisov[5], Alexander Gerbershagen[6], Sylvain Girod[1], Fabrice Malacrida[1], Pedro Manuel Mendes Correia[4], Fabian Metzger[7], Marcia Quaresma[8], Catarina Quintans[8], Maarten Van Dijk[1], Heinz Vincke[1], Pavol Vojtyla[1]

[1]CERN, Geneva, Switzerland
[2]University of Illinois, Urbana, IL, USA
[3]EPFL, Lausanne, Switzerland
[4] University of Aveiro, Aveiro, Portugal
[5]INFN, Torino Section, Torino, Italy
[6]PARTREC, Groningen, Netherlands
[7] Helmholtz-Institut für Strahlen- und Kernphysik, Bonn, Germany
[8]LIP, Lisbon, Portugal
[*]claudia.ahdida@cern.ch

In the context of the Physics Beyond Colliders Project, a QCD facility named AMBER/NA66 was developed as a successor of the COMPASS experiment. AMBER is located in the surface hall EHN2 in the CERN SPS North Area. The approved physics program of AMBER includes, amongst others, measurements of the pion-induced Drell-Yan process. This process shall be studied with a high-intensity 190 GeV/c pion beam impinging on a tungsten and several carbon targets followed by a 2.2 m long absorber. A total of 3.07×10^{14} pions on target per year shall be reached. This corresponds to a beam intensity increase by 68% with respect to the latest COMPASS Drell-Yan run in 2018. During the latter, the annual net ambient dose equivalent at the nearby environmental monitoring station close to the CERN fence reached 75% of the annual limit of 1 mSv. A radiation survey inside of the EHN2 hall and in its vicinity further allowed identifying several locations with elevated radiation levels.

To increase the beam intensity delivered to EHN2 while staying compliant with CERN's radiation protection code regarding doses to the personnel and members of the public, detailed studies for improving the shielding around the AMBER target area and along the M2 beam line were performed. These studies include the evaluation of the prompt dose rates in the accessible areas of EHN2 and next to it, at the CERN fence, and at the surrounding publicly accessible places. In addition, the residual dose rates inside of the target area were evaluated for different cooling times to determine adequate access requirements. Finally, the air activation inside the EHN2 hall and the exposure of members of the public due to air releases into the environment were assessed. The studies were performed with the FLUKA Monte Carlo particle transport code and the ActiWiz Creator tool.

2.1. Introduction

Within the Physics Beyond Colliders initiative, new opportunities offered by the existing CERN accelerator complex and scientific infrastructures are being studied that are complementary to high-energy colliders. One of the experimental areas offering great potential for such new projects is the SPS North Area. Several possible future projects have been proposed for the experimental areas EHN1, EHN2 and ECN3. One of them is AMBER, a new QCD facility succeeding the COMPASS experiment in EHN2 (Adams et al., 2019). The initial phase-1 of AMBER was approved and it will start in 2023. This phase

will last until after 2030 and it shall include three main topics: (1) Measurements of the antiproton production cross sections, (2) measurements of the proton radius, and (3) cross-section measurements of the pion-induced Drell-Yan process.

From an RP point of view, the Drell-Yan run is the most critical in view of the 190 GeV/c high intensity negative pion beam of 1×10^9 particles/spill and an annual intensity on target of 3.07×10^{14} (see Table 2.1). Such an annual intensity is 68% higher than the maximum intensity reached for past COMPASS Drell-Yan runs during which already increased radiation levels were observed.

Table 2.1. Key beam parameters for the AMBER Drell-Yan program

Momentum	190 GeV/c
Particle type	Negative pions
Beam intensity on target per spill	1×10^9
Spill duration	4.8 s
Cycle length	15 s
Annual particles on target (POT)	3.07×10^{14}

The goal was therefore to perform a design optimization of AMBER to cope with its future high intensity Drell-Yan runs. The ALARA approach was followed in line with CERN's radiation protection code (CERN, 2006). The design optimization includes detailed studies of the prompt and residual radiation, air activation and the environmental radiological impact. The studies were performed with the FLUKA Monte Carlo particle transport code (Ahdida et al., 2022; Battistoni et al, 2015; FLUKA.CERN, 2022) and the ActiWiz Creator tool (Vincke, 2014).

2.2. Past COMPASS Drell-Yan runs

In the past, COMPASS conducted two pion-induced Drell-Yan runs. During these runs an increased annual dose was observed at the CERN fence that is approximately 80 m far from EHN2 (see Figure 2.1). At the most critical location of the fence, the environmental monitoring station SMS824 is located. During the 2015 run with 1.7e14 POT it registered a neutron annual ambient dose equivalent of 745 µSv thus already reaching 75% of the annual ambient dose equivalent limit of 1 mSv at the CERN fence.

For the 2018 run, efforts were therefore made to improve the shielding around the COMPASS target and absorber, which was however challenging due to the space constraints coming from the equipment needed for the polarized target that COMPASS was using. Only shielding lateral to the target area could be slightly reinforced allowing increasing the intensity by 10%. In 2018, the integrated net ambient dose equivalent reached again 75% of the annual limit defined for CERN boundaries.

Figure 2.1. Aerial view of EHN2 and the position of the closest stray radiation monitoring station SMS824 located at the CERN fence.

SMS824 is located on the SE side of EHN2 referred to as the Salève side. The NW side is referred to as Jura side.

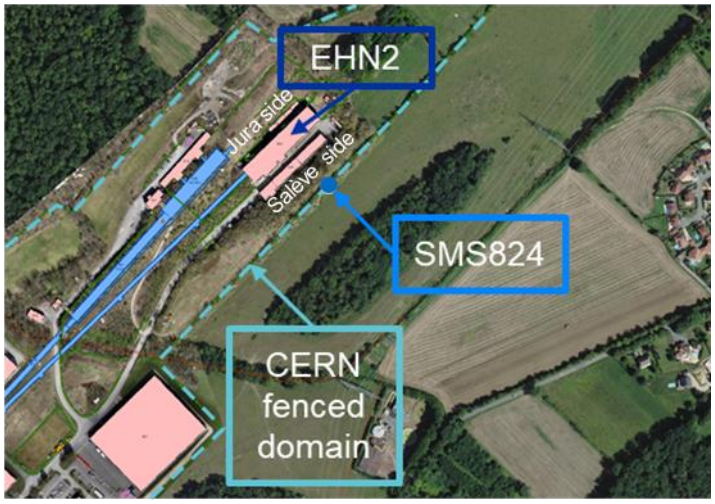

During the 2018 COMPASS run, two radiation surveys were performed as well in order to map the dose rates in the accessible areas inside and next to EHN2 in more detail. The surveys revealed several locations close to the beamline region with dose rates not compliant with the given area classification. EHN2 is classified as a Supervised Radiation Area with low occupancy (15 µSv/h limit), while the freely accessible area outside of EHN2 is classified as a Non-designated area (2.5 µSv/h limit), both with low occupancy (see Figure 2.2).

Figure 2.2. Radiation Area classification at CERN (CERN, 2006).

	Area	Annual dose limit (year)	Ambient dose equivalent rate		Airborne activity concentration	Surface contamination	
			permanent occupancy	low occupancy			
	Non-designated	1 mSv	0.5 µSv/h	2.5 µSv/h	0.05 CA	1 CS	
Radiation Area	Supervised	6 mSv	3 µSv/h	15 µSv/h	0.1 CA	1 CS	
	Simple Controlled	20 mSv	10 µSv/h	50 µSv/h	0.1 CA	1 CS	Controlled Area
	Limited Stay	20 mSv	-	2 mSv/h	100 CA	4000 CS	
	High Radiation	20 mSv	-	100 mSv/h	1000 CA	40000 CS	
	Prohibited	20 mSv	-	> 100 mSv/h	> 1000 CA	> 40000 CS	

CA: Guidance value for chronic occupational exposure to airborne activity. Exposure to an airborne activity concentration of CA for 40 hours per week and 50 weeks per year yields a committed effective dose of 20 mSv (Swiss RPO, 2017).
CS: Guidance value for surface contamination.

2.3. FLUKA model of AMBER

A detailed FLUKA model of the experimental setup of AMBER in EHN2, including its upstream beamline and surrounding ground profile, was developed and optimized.

The beam transfer tunnel TT84 with the full beamline starting from collimator 5 that is approximately 270 m upstream of the AMBER target was implemented in FLUKA using FLAIR (Vlachoudis, 2009) (see Figure 2.3). The model includes the collimators, the CEDAR counters for particle identification as well as the various magnetic elements of the beamline. The respective magnetic fields were modelled for each magnet. Furthermore, a dedicated source routine was used to define the momentum, position and angular distribution at collimator 5 according to distributions resulting from calculations using the HALO program (Iselin, 1974).

For EHN2, the model includes the beamline in the upstream part followed by the AMBER target area and then the AMBER experimental area in the downstream part. The large advantage for the target area shielding design is that AMBER uses simple solid targets made of tungsten and carbon, which do not require the complex cooling infrastructure as it was the case for the COMPASS polarized target. This allows placing a massive concrete shielding bunker of 7.2 m in height and 6.4 m in width around this critical area. Access to the bunker is provided via an access chicane. Downstream of the targets, a 2.2 m long absorber (width/height = 110 cm) with a tungsten core (Ø = 4.75 cm) encompassed by aluminium oxide and stainless steel is located, which is further surrounded by iron shielding followed by the concrete shielding of the bunker.

Next to that, the shielding in the EHN2 beamline part, where elevated dose rates were measured during the 2018 RP surveys, was improved. The improvements include a shielded access chicane instead of the current straight access path as well as shielding reinforcements at the level of a cable passage.

Figure 2.3. FLUKA geometry generated with FLAIR.

Beam transfer tunnel TT84 including its beamline component.

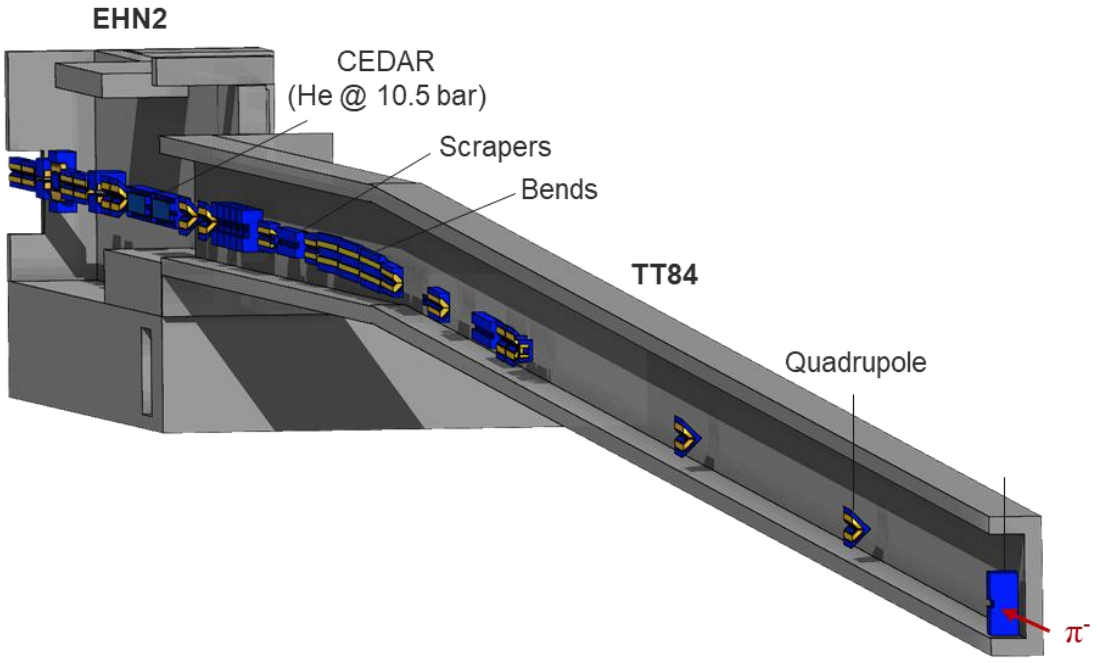

New shielding bunker around AMBER target area

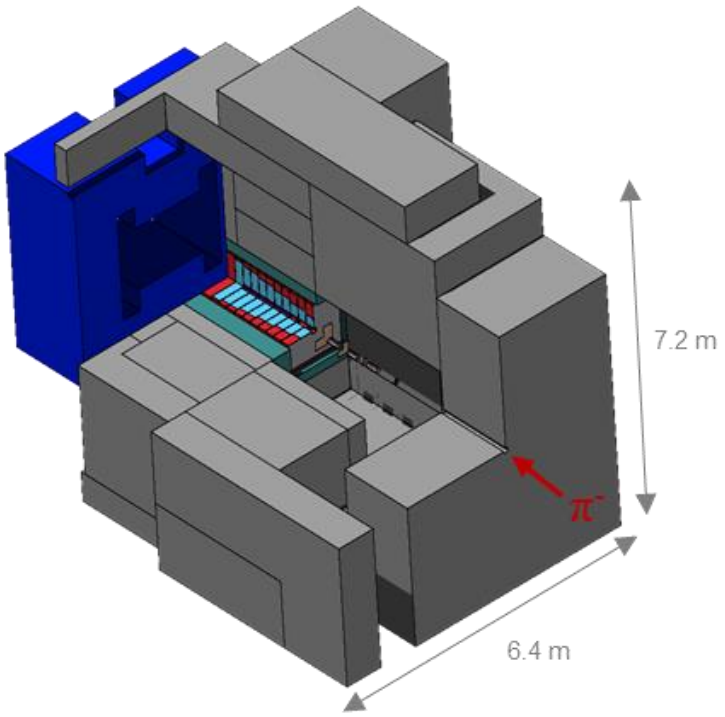

Finally, the surroundings of EHN2 were taken into account with modelling the ground profile according to data from CERN's geographic information system and technical drawings. The air volume above the ground is reaching up to 5 km in height.

The coordinate system adopted in the model is a right-handed Cartesian system with the *x*-axis pointing towards the Jura side of EHN2 (see Figure 2.2), the *y*-axis pointing vertically and the *z*-axis lying in direction of the beam line in EHN2. The most upstream target is located a 27090 cm in *z*.

2.4. Results

2.4.1. Prompt radiation

Figure 2.4 illustrates the prompt ambient dose equivalent rate in the transfer tunnel TT84 as well as in the beamline of the upstream part of EHN2. The results were normalized to the maximum beam intensity on the target of 1×10^9 pions per spill with 240 spills per hour. Approximately 11% of the beam is lost in the transfer tunnel TT48. As expected, the major part of the losses occurs at the collimators and scrapers of the beamline, which are designed to remove the undesired beam halo. The dose rates in the transfer tunnel TT84 reach up to a few tens of mSv/h at the worst locations, while they drop below 1 mSv/h in the surrounding soil.

Furthermore, the dose rates originating from losses in the beamline part that is located inside EHN2 were investigated. The dose rates up to the target bunker are shown in Figure 2.4. Less than 1% of the beam losses take place in the EHN2 part of the beamline, which is only partly shielded towards the top. From the downstream side of the target bunker, some radiation leakage is visible. The shielding could not be further reinforced in view of space constraints due to detectors located downstream.

The overall beam losses in the beamline were considered when normalizing the dose rates to obtain the actual beam intensity delivered to the target.

Figure 2.4. Side view of prompt ambient dose equivalent rate (in µSv/h) in the transfer tunnel TT84 (left) and in the upstream part of EHN2 including the (AMBER) target bunker (right).

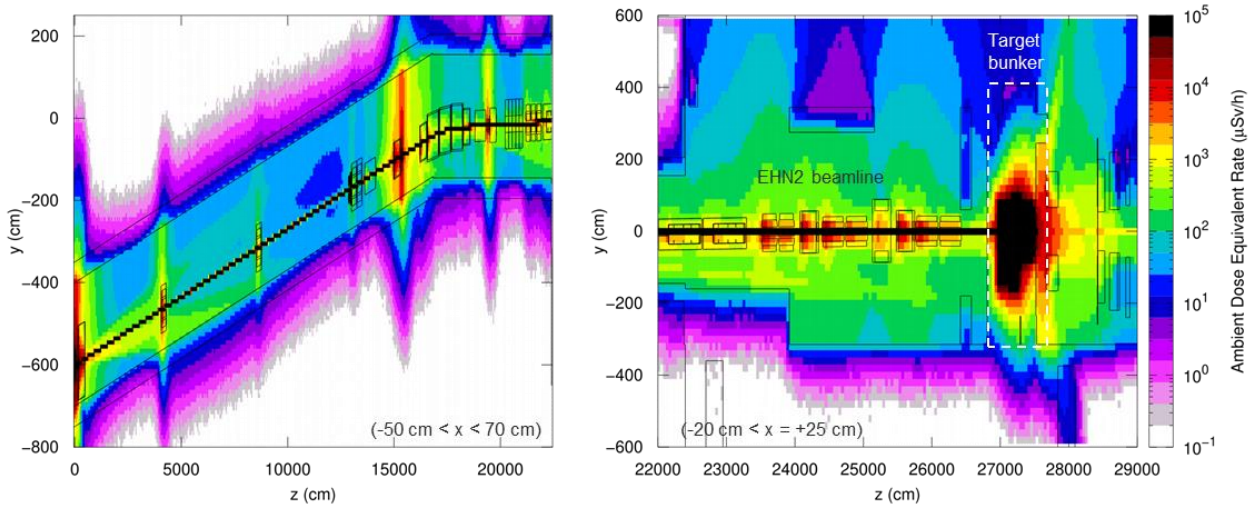

The dose rate distribution in EHN2 and its close vicinity is shown in Figure 2.5. It shall be noted that the Jura side of EHN2 is not accessible during beam operation. The dose rates inside the target bunker reach up to a few Sv/h close to the targets and absorber but they are significantly reduced by the surrounding shielding bunker. Also in the beamline region, the dose rates are well reduced by the new access chicane and the improved shielding on the Salève side of the beamline. When comparing the dose rates to the respective radiation area classification limits of a Supervised Radiation Area inside EHN2 and a Non-Designated Area on the Salève side of the building, it is demonstrated that the dose rates are well within the limits of the given area classification.

Figure 2.5. Top view of prompt ambient dose equivalent rate (in µSv/h) in EHN2 (left) with the colour scale according to the area classification (right).

The Jura side of EHN2 inside and outside of the building is not accessible during beam operation. The EHN2 hall is illustrated by the dashed line.

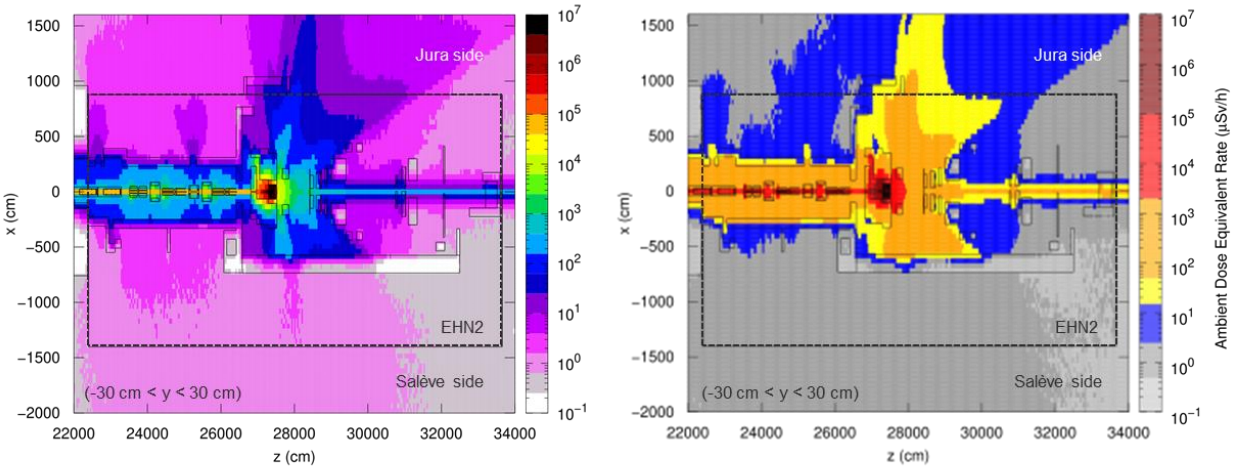

2.4.2. Residual radiation

The residual dose rates were evaluated assuming 6 months of irradiation with the maximum number of 3.07×10^{14} protons on target per year. Various decay times, namely 2 minutes, 10 minutes, 30 minutes, 1 hour, 3 hours, 1 day, 3 days, 1week, 1 month, 6 months, and 1 year, were investigated. The resulting dose rates inside the target bunker are shown in Figure 2.6 according to the area classification for 2 minutes of cool-down time. The latter corresponds to the minimum time allowed by the access system to enter the area. It can be seen that close to the targets and the absorber, the dose rates clearly exceed the 15 µSv/h limit of the usual classification of a Supervised Radiation Area. The dose rate plot for the working position, i.e. at 40 cm of distance from the beamline, reveal that the Supervised Radiation Area limit is surpassed for decay times shorter than 1 day and that the 50 µSv/h limit of a Simple Controlled Area is exceeded for less than 10 minutes of cool-down. This allows defining the required area classification and access constraints. To monitor the residual dose rates inside the area, an ionization chamber will be installed inside the shielding bunker.

Figure 2.6. Residual ambient dose equivalent rate (in µSv/h) inside the AMBER target bunker after 2 minutes cool-down (left) and for different cool-down times at 40 cm distance from the beamline axis (right).

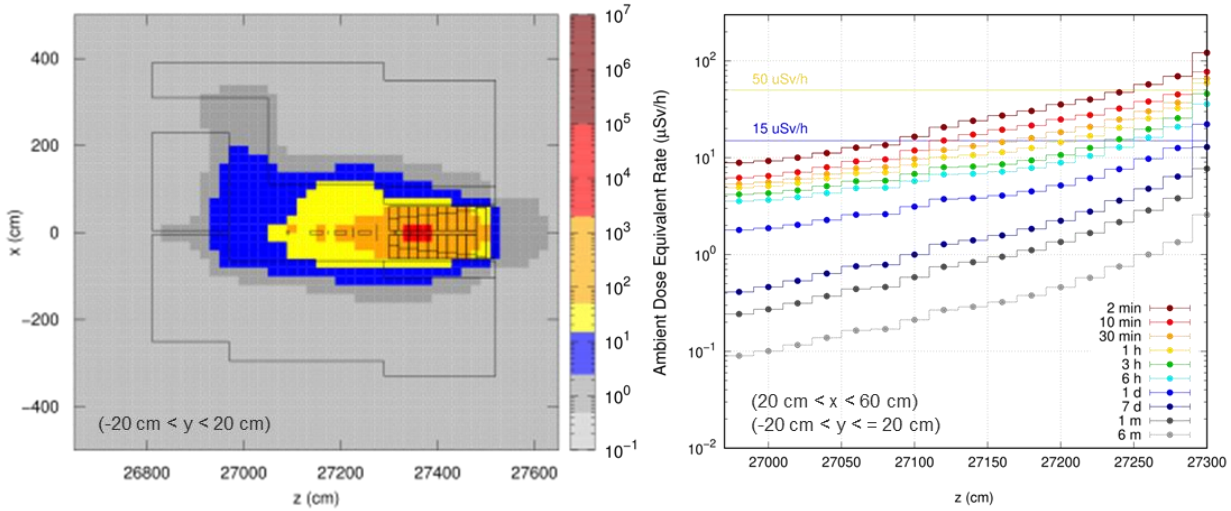

2.4.3. Skyshine radiation

The skyshine radiation was studied for the large-scale surrounding of EHN2 including the CERN fence and the adjacent publicly accessible area. For all areas, reference points where exposure of the personnel and public might be of concern as well as the locations of the environmental monitors at the CERN fence were chosen. These points include the hill on the Jura side and the road on the Salève side of EHN2 for the personnel, and a garden and the nearest house in the neighbouring residential for the public.

Table 2.2 summarizes the calculated annual effective doses at the reference points inside and outside the CERN fenced domain. The given conservative occupancy factors were taken into account for each point, respectively. The occupancy factors in public areas are based on international guidelines (IAEA, 2001) with the worst-case occupancy factor of 1 assumed for residential areas and 0.06 for gardens. No additional shielding factors (e.g. house walls) were conservatively assumed. The resulting annual effective doses reach 1 µSv/year and 2 µSv/year in the garden and at the nearest house location, respectively, and they are thus well below 10 µSv/year, wherefore the facility is considered as optimized (CERN, 2006). It shall be noted that contributions from other CERN sources at the given locations can be considered negligible. For the reference points inside the CERN fenced domain, a maximum of 53 µSv/year is obtained for the road on the Salève side of EHN2. This estimate is considered very conservative, since an occupancy of 20% is highly unlikely at the given place. The results demonstrate that the facility operation is justified and that the facility is well optimized with regards to the effective annual dose due to skyshine radiation.

Table 2.2. Annual effective doses (in µSv/year) for different reference points and the assumed occupancy factors. Statistical uncertainties are smaller than 10%.

Reference point	Annual effective dose (µSv/year)	Occupancy factor
Garden	1	0.06
Residential area	2	1
Hill on Jura side of EHN2	29	0.05*
Road on Salève side of EHN2	53	0.05*

*Low occupancy workplace (20% of permanent workplace occupancy factor of 0.23)

Table 1.3 gives the annual values of the annual doses calculated for the locations of the CERN stray radiation monitoring stations, for two simulated beam source terms. The first simulation considers the full source distribution from before collimator 5, while the second simulation uses a pencil beam source starting just before the target. The aim is to evaluate the contribution originated by the interaction of the beam with target and compare it to the results obtained with the full source distribution starting from before collimator 5. The monitoring station PMS824 has the shortest distance to EHN2 (~80 m) and is located laterally to it (see Section 1.2). PMS821 and PMS822 are located on the downstream Jura side of EHN2 at distances of approximately 140 m and 260 m, respectively. PMS823 is downstream of EHN2 at the longest distance of 360 m. As expected, at the position of PMS824 the annual ambient dose equivalent would be at highest namely 258 µSv/year, which lies well below the 1 mSv/year annual limit at the CERN fence and beyond (CERN, 2006).

Table 2.3. Annual dose (in µSv/year) at monitoring stations at the CERN fence. No occupancy is taken into account. Statistical uncertainties are smaller than 10%.

Values are given for the beam starting at collimator 5 (full source) and in front of the target (target only).

Monitoring station	Annual dose (µSv/year)	
	Source from collimator 5	Source from target only
PMS821	105	70
PMS822	17	10
PMS823	7	4
PMS824	258	165

Next to the simulation including the losses in the upstream beamline, a separate simulation was performed, in which the beam was starting directly in front of the target inside the shielding bunker. This allowed evaluating the contribution of the beam losses to the overall skyshine radiation. It was found that particularly for the far locations, the contribution of the losses in the beamline was significant, up to 50%. This can be explained by the fact that most of the beamline is not shielded and high-energy neutrons are not attenuated, as it is the case for the shielding bunker.

2.4.4. Air activation

The air activation in the target bunker region and the rest of the EHN2 hall was evaluated assuming a 6-month irradiation time with a total of 3×10^{14} POT. The production of radionuclides in each region was calculated from particle fluence values by using ActiWiz and considering all the relevant short- (e.g. ^{11}C, ^{13}N, ^{14}O, ^{15}O and ^{41}Ar) and long-lived radionuclides (e.g. ^{3}H, ^{7}Be, ^{14}C, ^{32}P, ^{33}P, ^{35}S). It was conservatively assumed that there was no decay time nor mixing nor extraction of air. The total activity concentrations in air for both regions are given in Table 2.4 with a higher value for the target bunker region that amounts to 1 kBq/m^3. When comparing to the Swiss CA[1] values, the airborne activity in both regions is well below the CERN limit of 0.1 CA (see Figure 2.2) and giving rise to an inhaled dose of maximally 0.02 μSv per hour of stay.

Table 2.4. Air activation in the target bunker region and the rest of the EHN2 hall.

Air region	Total activity concentration (Bq/m^3)	Multiple of CA*	Inhaled dose for 1 hour of stay
Target bunker	1000	2E-02	2E-02 μSv
EHN2 hall	2	3E-05	<< 1 μSv

*See the definition in Figure 2.2.

Finally, the dosimetric impact on members of the public due to releases of activated air to the atmosphere was assessed using the methodology described in (Vojtyla, 2021). No decay of radionuclides from their creation points to a release point was conservatively assumed. In total 8.2 GBq of airborne radioactivity released continuously to the atmosphere during one year of operation would result in effective doses lower than 0.2 nSv. The main contributors would be the short-lived radioactive gases ^{13}N (48%), ^{11}C (22%), ^{41}Ar (12%), and ^{15}O (12%).

2.5. Summary and Conclusions

The Drell-Yan program of the AMBER experiment will involve a high-intensity hadron beam transferred to the EHN2 hall located at the surface. This configuration poses several radiation protection challenges particularly due to prompt dose rates in EHN2 as well as at the CERN fence. A comprehensive design optimization has therefore been performed with the FLUKA Monte Carlo particle transport code and the ActiWiz Creator tool. The optimization did not only focus on the target area, but also on the beamline region, where dose rate surveys during past COMPASS Drell-Yan operation with lower intensities revealed shielding weaknesses.

The AMBER design optimization included extensive shielding improvements allowing optimizing the prompt and residual radiation, air activation and the environmental impact. It included the introduction of a massive shielding bunker around the target area as well as shielding improvements at strategic beamline locations. The latter was important since the contributions from beam losses in the beamline to the dose equivalent in EHN2 hall were found to be non-negligible.

The present radiation protection assessment demonstrates that the optimized design will significantly improve the absorption of radiation inside the target area and reduce the prompt dose rates in the accessible areas inside and outside EHN2 to levels well below the limits of the given area classification. The studies of the residual dose rates inside of the shielding bunker defined the required area classification and access constraints for the

target area. Furthermore, the skyshine radiation was investigated proving that the facility was sufficiently optimized. Finally, the environmental impact was studied. It was found that it is dominated by skyshine radiation, while the exposure of members of the public due to air releases is negligible. It was shown that the effective dose to members of the public remains well below CERN's dose objective of 10 μSv/year.

2.6. List of references

Adams, B. et al. (2019), "COMPASS++/AMBER: Proposal for Measurements at the M2 beam line of the CERN SPS Phase-1", CERN-SPSC-2019-022

Ahdida, C. et al. (2022), New Capabilities of the FLUKA Multi-Purpose Code, Frontiers in Physics 9, 788253.

Battistoni, G. et al. (2015), "Overview of the FLUKA code", Annals of Nuclear Energy 82, 10-18.

CERN (2006), "SAFETY CODE F Rev. Radiation Protection".

FLUKA.CERN (2022), *FLUKA*, viewed 11 November 2022, https://fluka.cern

IAEA (2001), "Generic Models for Use in Assessing the Impact of Discharges of Radioactive Substances to the Environment, Safety Reports Series, IAEA-srs-19," IAEA, Vienna.

Iselin, C. (1974), "HALO: a computer program to calculate muon halo", CERN report, 10.5170/CERN-1974-017.

Swiss Radiological Protection Ordinance (RPO) (2017)

Vincke, H. and Theis, C. (2014), "ActiWiz – optimizing your nuclide inventory at proton accelerators with a computer code", Progress in Nuclear Science and Technology.

Vlachoudis, V. (2009), "FLAIR: A Powerful But User Friendly Graphical Interface For FLUKA", in Proc. Int. Conf. on Mathematics, Computational Methods & Reactor Physics (M&C 2009), Saratoga Springs, New York.

Vojtyla, P. (2022), "EdaraCpp: User and developer manual", CERN Internal report.

Vojtyla, P. (2021), "Models for assessing the dosimetric impact of releases of radioactive substances from CERN facilities to the environment – Air", CERN Internal report.

2.7. List of abbreviations and acronyms

CERN	Conseil Européen pour la Recherche Nucléaire
AMBER	Apparatus for Meson and Baryon Experimental Research
CEDAR	Cherenkov Differential Counter with Achromatic Ring Focus
COMPASS	Common Muon and Proton Apparatus for Structure and Spectroscopy
QCD	Quantum Chromodynamics
SPS	Super Proton Synchrotron
RP	Radiation Protection

3. Sensitivity study of elements for neutron deep penetration in concrete

Hiroshi IWASE[1*], Ken-ichi KIMURA[2], Mohd Faiz Mohd ZIN[34], Yasuhito SAKAKI[1], Yoshihito NAMITO[1], and Hideo HIRAYAMA[1]

[1] High Energy Accelerator Research Organization (KEK), 1-1 Oho Tsukuba, Ibaraki, Japan,
[2]Fujita Cooperation, Ono 2025-1, Atsugi 243-0125, Japan,
[3] The Graduate University for Advanced Studies, SOKENDAI, Hayama 240-0193, Japan,
[4] (present address) Malaysian Nuclear Agency, 43000 Kajang, Selangor, Malaysia
[*] hiroshi.iwase@kek.jp

The sensitivity of elements in normal concrete to neutron attenuation was investigated. This study corresponds to a part of the search of a standard concrete composition. This study suggests that neutron deep penetration in normal concrete does not depend on the composition of the concrete, but on its density and hydrogen (or water) content.

3.1. Introduction

Concrete is the primary radiation shielding material, and huge amounts of concrete are used in accelerators and radiation facilities. The total amount of concrete can affect the overall cost. On the other hand, many shielding designs are performed with common concrete compositions, which require a reduction in the total density of the concrete to ensure an adequate safety margin. It would be ideal if a standard concrete composition could be defined that could be universally used for neutron shielding calculations in any region of the world. First, it is necessary to check for the presence of elements that give high sensitivities to the results. In this study, sensitivity of elements to the attenuation of neutron deep penetration in normal concrete is investigated.

3.2. Methods

Neutron attenuation in concretes were calculated by PHITS [Sato 2018]. The initial neutron energy is 100 MeV in this study. The evaluated nuclear data of JENDL-HE2007 (the upper limit of the data library is 150 MeV) [Watanabe 2011], was used for the neutron transport calculation. Neutron doses behind different thick concretes were calculated as shown in Figure 3.1. Neutron energy spectra were tallied by the track length method in a thin disk air region placed behind concrete with a radius of 10000 cm. The results were converted into neutron doses using the conversion factor of the effective dose of the AP condition.

Figure 3.1. Geometry of the calculation

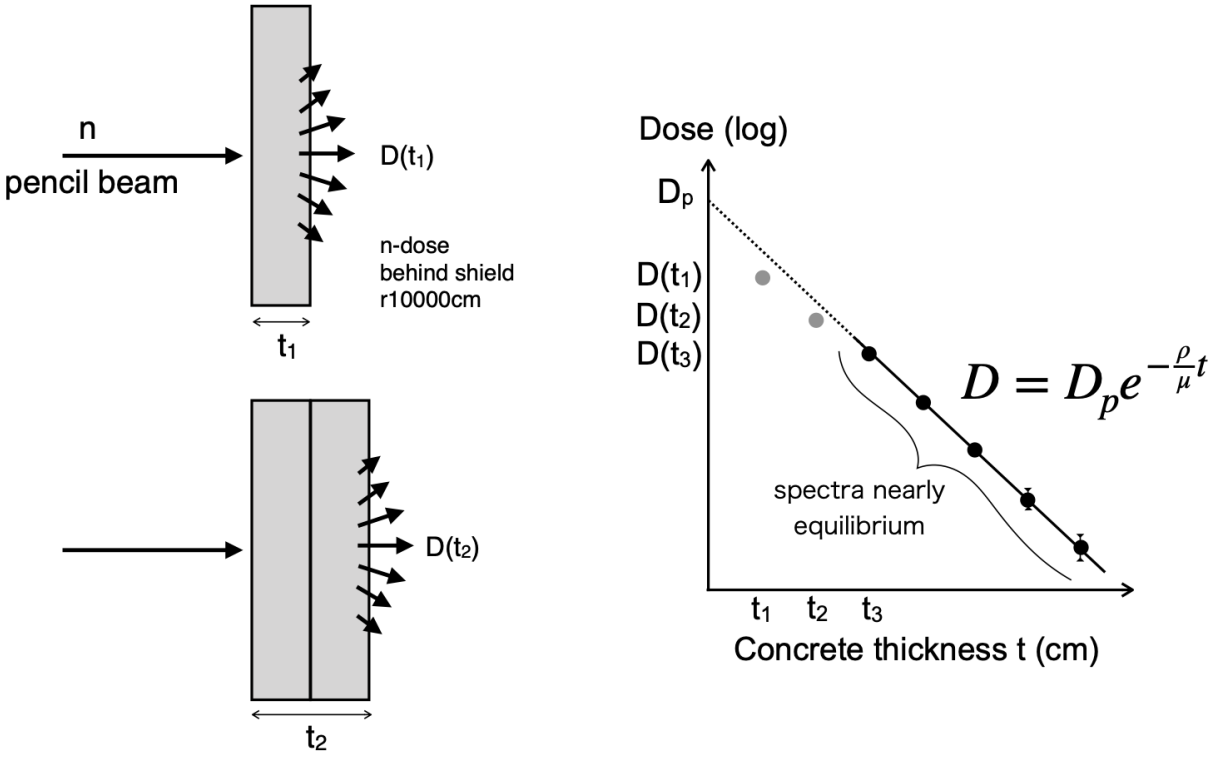

3.3. Concrete compositions

Several concrete compositions are chosen from the material data book for Monte Carlo calculation [McConn 2011]. In this study only the normal density concretes are discussed. (i.e., heavy concretes are not discussed). Table 3.1 is the list the selected concretes. The number for each element in the table is the atom density divided by 10^{24} (/cm^3).

Table 3.1. Concrete compositions 1/2

	Conc.81 Hanford Dry	Conc.82 Hanford Wet	Conc.86 MCNP	Conc.94 ORNL	Conc.95 Ordinary (NBS 03)	Conc.96 Ordinary (NBS 04)
H	0.005210	0.017282	0.006090	0.008502	0.011914	0.007804
C				0.02020	0.00590	
O	0.03956	0.04541	0.04341	0.03551	0.04188	0.04406
Na	0.00012	0.00012	0.00090	0.00002		0.00105
Mg	0.00076	0.00076		0.00186	0.00141	0.00015
Al	0.00338	0.00336	0.00179	0.00056	0.00189	0.00240
Si	0.01297	0.01291	0.01739	0.00170	0.00731	0.01588
S					0.00013	0.00006
K	0.00044	0.00044		0.00004	0.00006	0.00070
Ca	0.00263	0.00262	0.00196	0.01110	0.00872	0.00293
Ti						
Cr						
Fe	0.00135	0.00134	0.00033	0.00019	0.00028	0.00031
Density ρ (g/cm^3)	2.18	2.35	2.25	2.30	2.35	2.35
Water density ρ_{H2O} / ρ x 100 (%)	3.57	10.99	4.04	5.53	7.58	4.96

Table 3.1. Concrete compositions 2/2

	Conc.97 Ordinary (NIST)	Conc.98 Portland	Conc.99 Regular	Conc.100 Rocky Flats	Conc.101 Serpentine
H	0.030369	0.013742	0.013742	0.010396	0.019961
C	0.00029	0.00012		0.00642	0.00010
O	0.04977	0.04581	0.04606	0.04234	0.04046
Na	0.00092	0.00096	0.00175	0.00038	0.00023
Mg	0.00007	0.00011		0.00072	0.00702
Al	0.00102	0.00174	0.00175	0.00112	0.00090
Si	0.01502	0.01662	0.01662	0.00771	0.00942
S				0.00008	
K	0.00036	0.00046		0.00049	0.00013
Ca	0.00148	0.00152	0.00152	0.00802	0.00215
Ti				0.00003	
Cr					0.00002
Fe	0.00016	0.00035	0.00035	0.00025	0.00070
Density ρ (g/cm^3)	2.30	2.30	2.30	2.32	2.10
Water density ρ_{H2O} / ρ x 100 (%)	19.73	8.93	8.93	6.70	14.21

3.4. Neutron attenuation in different concretes

The results are shown in Figure 3.2-(A). Neutron attenuation is different for each concrete since its composition and density are different from others. Figure 3.2-(B) shows another plot of concrete thickness corrected for density, i.e. concrete thickness is expressed by the areal density. Results are more consistent, but there are still sufficient disagreement. It indicates that the difference in Figure 3.2-(A) is not due to density. Similar check is done by Figure 3.2-(C) by correcting the concrete thickness by the mean free path. It is noted that the mean free path, the inverse value of the macroscopic total cross section, is calculated for the incident energy in this study. In this plot the thickness can be considered approximately how many times neutron scatters in the concrete. It shows still certain amount of discrepancy. It argues that the neutron attenuation in concrete is not determined simply by the number of scatterings. It implies that the different elements may have different contributions to the neutron attenuation in concrete.

Figure 3.2. Calculation results of the neutron attenuation in different composition normal concretes. The same results with the normalization of the concrete thickness by its density and mean free path are additionally shown.

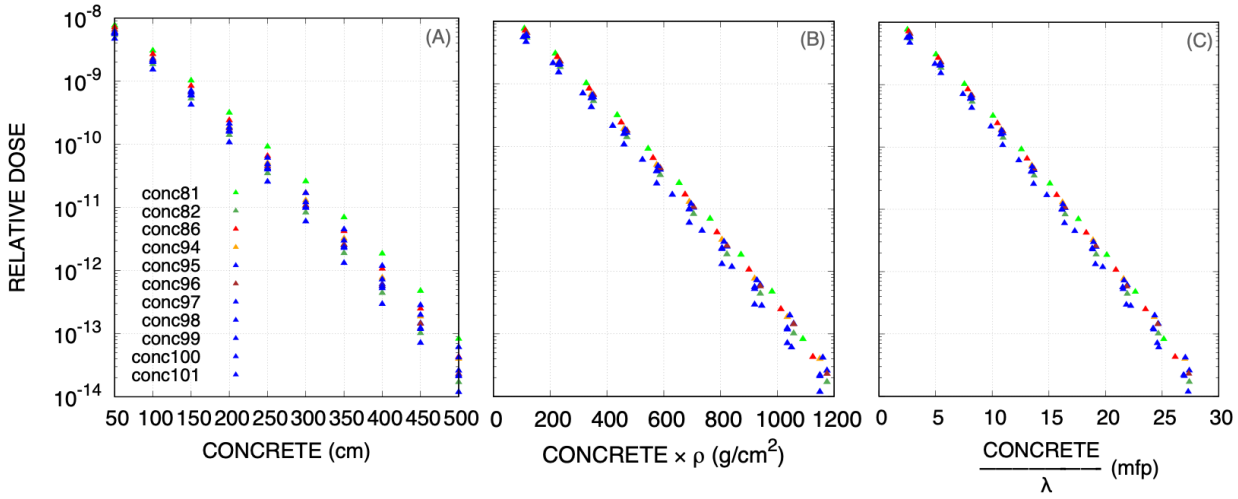

3.5. Sensitivity study on neutron attenuation in concrete excluding a single element

The contribution of each element to the neutron attenuation in concrete is tested. Several test concrete compositions are prepared by excluding one element from a specific composition (firstly it is the conc. 81 in Table 3.1). The test compositions and their densities are shown in Table 3.2. In the table, item name of "con81excl.H" is one of the test concrete excluding hydrogen from the original composition. Figure 3.3-(A) show the results. The curve of excl.O shows the highest dose, and the next is excl.Si. From this result, it seems that oxygen and silicon are the key elements due to such weak attenuations by being excluded. However it is substantially not true. Figure3.3-(B) shows the same results plotted by the thickness of the areal density. The result shows that all the attenuation curves show almost the same in both value and gradient excepting hydrogen. It indicates that only hydrogen has higher contribution than the other elements for neutron attenuation in this

concrete. Same test was performed for concrete 86 and the tendency was quite same with Fig 3.3-(B). Even the test was not performed for the other concretes, the results suggest that content of elements other than hydrogen is independent for neutron attenuation in concrete in case it is evaluated with considering its density. On the other hand, the hydrogen (or practically water) content should be treated separately from the density. It means; in case to start a neutron shielding calculation with using normal concrete, choosing a composition of concrete is not important but its density and the water content should be the key parameters.

Figure 3.3. Neutron attenuation in concrete excluding the specific element.

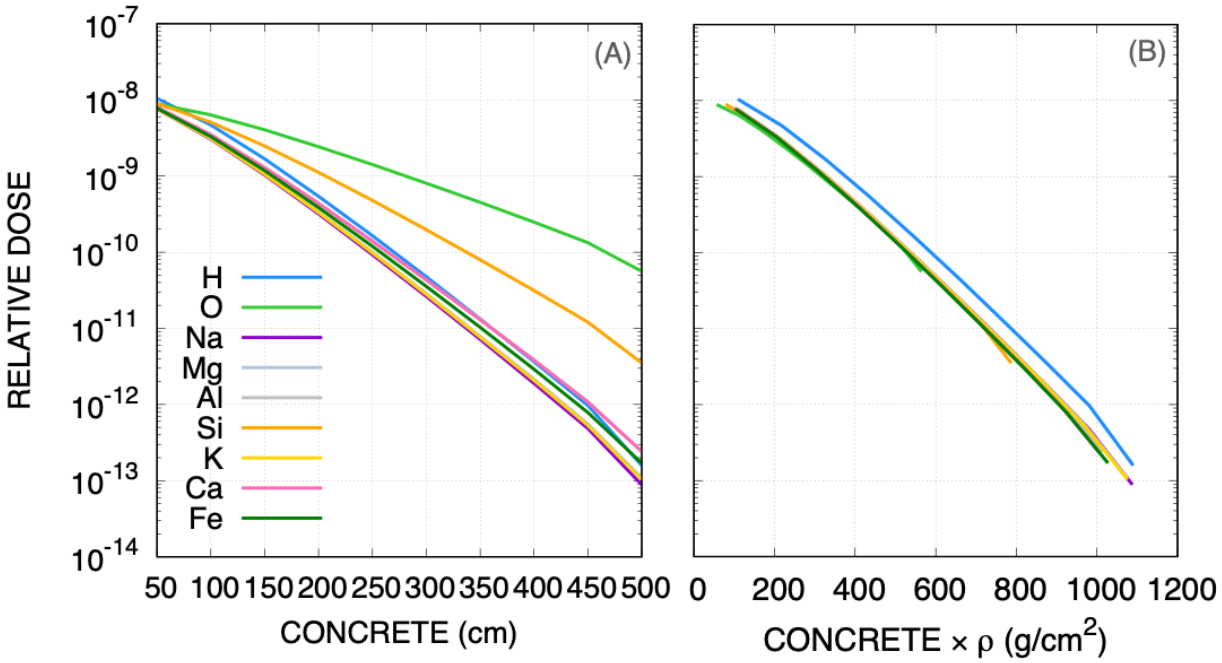

Table 3.2. Concrete compositions for the sensitivity study

	Con81excl.H	Con81 excl.O	Con81 excl.Na	Con81 excl.Mg	Con81 excl.Al	Con81 excl.Si	Con81 excl.K	Con81 excl.Ca	Con81 excl.Fe
H		0.00521	0.00521	0.00521	0.00521	0.00521	0.00521	0.00521	0.00521
O	0.03956		0.03956	0.03956	0.03956	0.03956	0.03956	0.03956	0.03956
Na	0.00012	0.00012		0.00012	0.00012	0.00012	0.00012	0.00012	0.00012
Mg	0.00076	0.00076	0.00076		0.00076	0.00076	0.00076	0.00076	0.00076
Al	0.00338	0.00338	0.00338	0.00338		0.00338	0.00338	0.00338	0.00338
Si	0.01297	0.01297	0.01297	0.01297	0.01297		0.01297	0.01297	0.01297
K	0.00044	0.00044	0.00044	0.00044	0.00044	0.00044		0.00044	0.00044
Ca	0.00263	0.00263	0.00263	0.00263	0.00263	0.00263	0.00263		0.00263
Fe	0.00135	0.00135	0.00135	0.00135	0.00135	0.00135	0.00135	0.00135	
Density ρ (g/cm^3)	2.17	1.13	2.18	2.15	2.03	1.58	2.15	2.01	2.06

3.6. Water content and neutron attenuation in concrete

The suggestion in the previous section implies that neutron attenuation in the normal concrete does not change if its density and hydrogen (or practically water) content are same. Figure 3.4 shows neutron attenuation curves in the different concretes in a condition that the water content is set to the same value of 4% in the weight density (ca. average in Table 3.1) each other. Figure 3.4-(A) shows the result and there is discrepancy between the different concretes. It is due to the different densities of the concretes. On the other hand the final result of Figure 3.4-(B) shows quite good agreement each other. This result insists that the neutron attenuation in the normal concrete should be able to be determined by its density and water content.

Figure 3.4. Neutron attenuation in different concretes, with modification of a same water content of 4% (wt.)

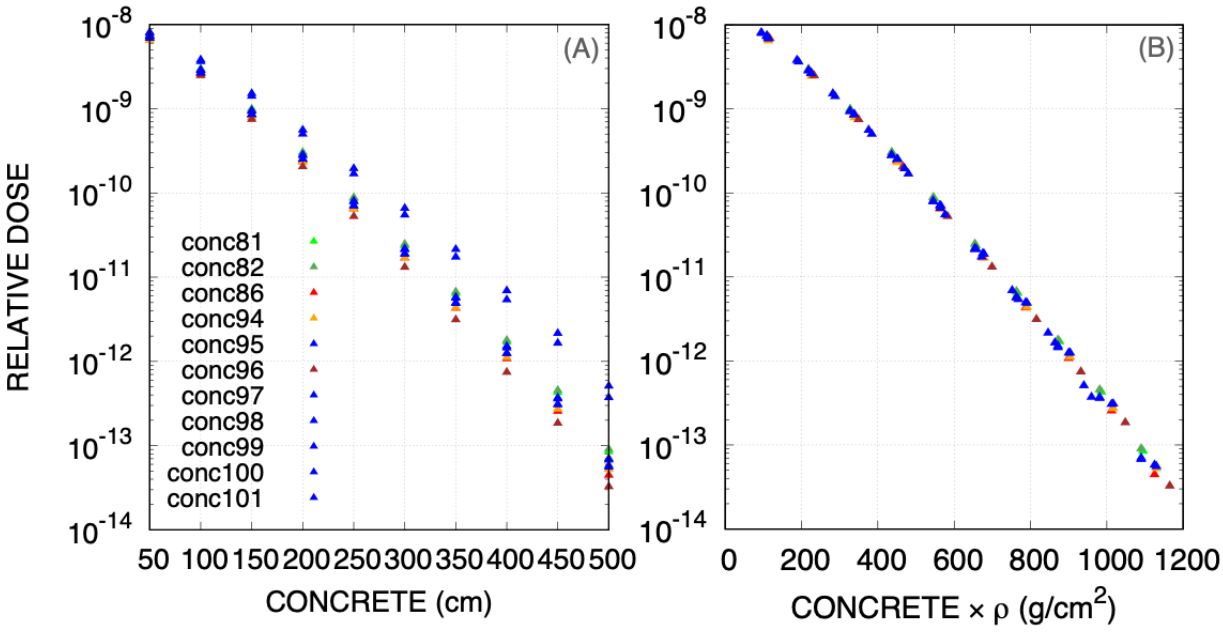

3.7. Summary and Conclusions

This study is an initial step in the search for a standard concrete composition. Attenuation of 100 MeV neutron in normal concrete was investigated. The neutron attenuations in different composition concretes agree fairly well by considering its density, or by plotting as the thickness divided by the mean free path, but there are still discrepancies. Then the contribution of each element to the attenuation was examined, and it was confirmed that the contribution of hydrogen was significant, while the other elements were about the same in case the attenuation is compared in the concrete thickness of areal density. In terms of deriving standard composition of concrete for neutron attenuation, this study suggests only the density and hydrogen (practically water) content are important and the composition of elements other than hydrogen is independent to result. This discussion is not confirmed for other neutron energies and for heavy concretes. Further systematic study is required in the search for a standard concrete composition.

1.5.List of references

RJ McConn Jr, CJ Gesh, RT Pagh, RA Rucker, RG Williams III (2011). Compendium of Material composition data for radiation transport modeling, revision 1. PIET-43741-TM-963, PNNL-15870 Rev.1

Sato, T., Iwamoto, Y., Hashimoto, S., Ogawa, T., Furuta, T., Abe, S. I., ... & Niita, K. (2018). Features of particle and heavy ion transport code system (PHITS) version 3.02. Journal of Nuclear Science and Technology, 55(6), 684-690.

Watanabe Y., et al. (2011). Status of JENDL High Energy File, Journal of the Korean Physical Society, 59(2), 1040-1045.

3.8. List of abbreviations and acronyms

PHITS Particle and Heavy Ion Transport code System

JENDL Japanese Evaluated Nuclear Data Library

4. ARI-SXN beamlines radiation shielding analysis

R. S. Augusto[1*], D. M. Bacescu[1], O. Chubar[1], C. Schaefer[1], R. Lee[1], A. L. Walter[1]
[1]Brookhaven National Laboratory, Upton, NY 11973-5000, United States of America
[*]rdossanto@bnl.gov

ARPES and RIXS Imaging (ARI) and Soft X-ray Nanoprobe (SXN) are a pair of soft x-ray beamlines under development at the National Synchrotron Light Source II (NSLS-II), in the framework of the National Synchrotron Light Source Experimental Tools Two (NEXT-II) project, which is funded by the United States Department of Energy, Office of Basic Energy Sciences. Each beamline will have two branches that will be provided with soft x-rays from two elliptically polarizing undulators (EPU), with periods of 70 and 50 mm for ARI and SXN, respectively. These branch lines lead to end stations, where the x-rays will be utilized for research in various scientific domains.
In this work, the Monte Carlo (MC) particle transport and interaction code FLUKA was employed to generate and model the Gas Bremsstrahlung (GB) and Synchrotron Radiation (SR) throughout the beamlines. The shielding design process to keep chronic ambient dose equivalent rates as low as reasonably achievable (ALARA) on the experimental floor during operation will be detailed. Furthermore, a comparison with the analytical code STAC8 will be also provided for the SR. These simulation data are currently being used to validate the shielding design and the overall radiological framework in anticipation of the beamline's commissioning in 2027.

4.1. Introduction

The NSLS-II facility is a 3rd generation light source with a 3 GeV and 500 mA electron beam. It currently supplies synchrotron radiation to almost 30 beamlines with future development allowing for twice that capacity.

ARI and SXN are a pair of soft x-ray beamlines located in cell 29-ID of NSLS-II that are being constructed in the framework of the NEXT-II project. Each beamline will have two branches that will be provided with x-rays from two EPUs, with periods of 70 and 50 mm, respectively, for ARI and SXN. The two beamlines can operate independently and simultaneously. ARI's two branch lines run inboard and lead to either the angle-resolved photoemission spectroscopy (ARPES) or the resonant inelastic x-ray scattering (RIXS) end stations for research on the electronic structure variation in different materials with very low spatial resolution and very high photon fluxes. As for the SXN branch lines, running outboard, one branch will lead to a station for probing the structural and electronic characteristics of samples of interest with sub-10 nm spatial resolution. The second branch will be developed in the future. The ARI-SXN beamlines outside the tunnel are depicted in Figure 4.1.

Figure 4.1. Detailed 3D view of the ARI-SXN beamlines and surrounding areas, highlighting the ARI (red, inboard) and SXN (blue, outboard) beamlines as well as the FOE (yellow).

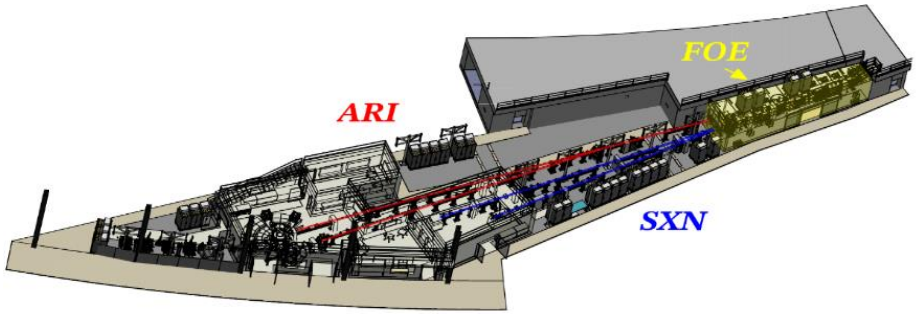

Source: Brookhaven National Laboratory

Shielding of the NSLS-II beamlines is designed to protect against GB and SR, as well as any secondary radiation generated. Those are chronic sources of radiation and the main contributors to dose rates outside of the shielding in normal operating conditions. As per the NSLS-II shielding policy guidelines, chronic ambient dose equivalent rates are to be kept ALARA and lower than 0.5 mrem h^{-1} (5 µSv h^{-1}) on contact with the downstream wall of the First Optical Enclosure (FOE) during regular operation. At 30 cm from the lateral wall and roof of the FOE, the shielding design goal is to achieve less than 0.05 mrem h^{-1} (0.5 µSv h^{-1}) on the experimental floor. Therefore, annual dose to staff and users is kept lower than 100 mrem (1 mSv) assuming a yearly occupancy of 2000 hours.

Exposure to personnel due to a fault event shall not exceed 20 mrem (200 µSv) in non-radiation-controlled areas or 100 mrem (1 mSv) in a radiation-controlled area. Shielding will be designed so that individual dose, integrated over the duration of the fault, does not exceed 20 mrem (200 µSv).

4.2. Gas Bremsstrahlung

The MC particle transport and interaction code FLUKA (Bohlen et al., 2014; Ferrari et al., 2005; Sala et al., 2022; Ferrari et al., 2022) version 2021.2.6 (http://www.fluka.org/) was employed to assess the GB shielding performance. For an accurate assessment of the radiation fields, it was necessary to model the source term, the FOE, and other beamlines' shielding–relevant elements.

As the 3 GeV electron beam traverses the 15.5 m straight section of the storage ring, GB is produced due to interactions with the residual gas. When the front-end safety shutters and photon shutter are open, GB will proceed into the FOE, generating secondary radiation as it interacts with the various beamline components.

The FOE is a lead shielding enclosure ~12 m long, whose inboard wall is slanted as it is juxtaposed to the storage ring accelerator enclosure. In this work, the FOE walls were uniformly modelled with lead thicknesses of 1.8, 1 and 5 cm for the lateral, roof, and downstream walls, respectively. The lateral walls are located at least 1.5 m from the beam centreline and the only openings considered were the two penetrations downstream, each of 25 cm diameter and partially protected with a guillotine. These guillotines consisted of stacked 40×40 cm lead panels, 10 cm thick and with a 10 cm diameter circular opening, attached to the inner side of the FOE wall.

The FOE connects to cabins downstream via 6 mm thick stainless steel beam transport pipes, which can be wrapped with extra shielding, if necessary. The end station cabins' walls and roof will be made of drywall and will not be part of the shielding configuration.

FLUKA was used to model the GB source, following a two-step methodology detailed in Ferrari et al (1993). A composition of H_2 (75%), 12.5% CO and 6.25% each of CO_2 and CH_4 (Marendziak et al., 2017; Sakhani et al., 2019), was assumed for the residual gas, considered to be at a pressure of 1 nTorr (~133 nPa). In this work, the GB source integrated power was 17 µW.

The shielding calculations featured various simulated GB scattering scenarios, including:

- normal operation – GB impinging onto scattering mirrors, assuming standard mirror configuration and an optimized shielding set up.
- maximum credible incidents – resulting from the full GB power impinging onto selected components and the subsequent secondary GB scattering.

The first category reflects a standard operation scenario; hence its results should be representative of chronic radiation exposure. The shielding geometry model included the main relevant radiation safety components, namely the glidcop masks and Bremsstrahlung collimator, as well as a tungsten white beam stop. A shielding optimization process resulted in the addition of both a lead panel and a GB stop to meet radiological requirements. The optimal configuration consisted of a 5-cm thick panel reinforcing the downstream wall, in a surface of 1 m × 75 cm, and a 32 cm × 24 cm × 16 cm lead GB stop just upstream of the downstream wall (see Figure 4.2).

The second category comprises fault cases which will be defined using ray tracing information to determine where and how the GB beam would more conservatively interact with the selected beam line elements, particularly missteer masks and the photon shutter. It should be noted that the likelihood of any of these maximum incidents is very low (hazard risk of H4). Other elements will be included in the calculation on an ad-hoc basis, depending on their potential shielding impact (e.g. likelihood of intercepting and significantly diverting the secondary GB). Since the ray tracing drawings are currently being prepared, 8 full beam loss scenarios, listed in Table 4.1, were specified using generic assumptions for both beam direction and fault location.

Figure 4.2. FOE detail in Flair GeoViewer (Vlachoudis, 2009) depicting the geometry used in the FLUKA simulation, including some selected components and a minimal shielding configuration proposed to meet radiological requirements during normal operation. Beam direction is to the right, outboard direction is up.

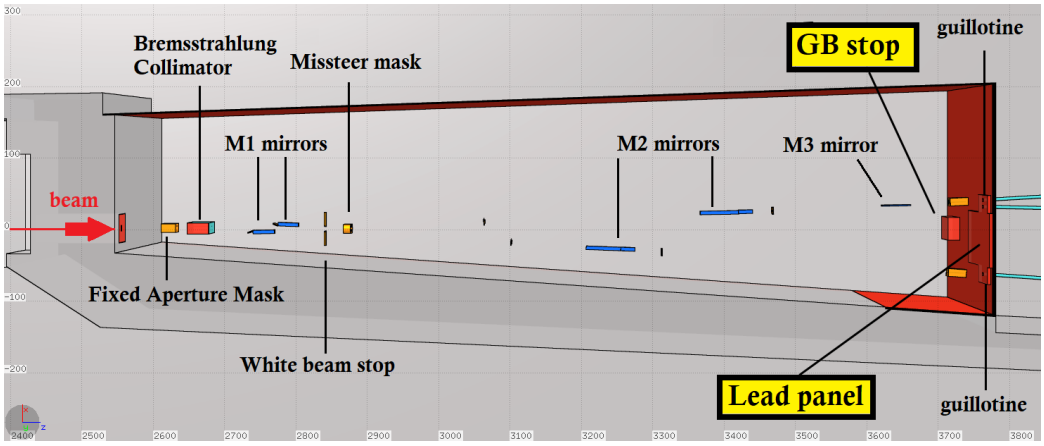

Source: Brookhaven National Laboratory

To confirm the adequacy of the FOE and transport pipes' shielding, maximum H*(10) values were scored outside of the FOE's roof, outboard and downstream walls, both at contact and at 30 cm. The maxima of neutron, gamma and beta contributions were also tallied. Biasing techniques were employed to inelastic interactions to optimize computation time.

Table 4.1. GB Maximum credible incidents analysed.

Case	Component	Director angle (x,y) [mrad]	Strike point (x,y,z) [cm]	Description
0	Fixed mask	*0,0*	*0, 0, 2606*	Direct impact on the fixed mask at its upstream face
1	Fixed mask	*1.333, 0.152*	*3.5, 0.4, 2626*	Shaving the fixed mask's outboard aperture
2	Fixed mask	*-1.066, -0.114*	*-2.8, -0.3, 2625*	Shaving the fixed mask's inboard aperture
3	Bremsstrahlung collimator	*1.324, 0*	*3.5, 0, 2645*	Missteered beam striking the collimator's outboard aperture
4	Bremsstrahlung collimator	*-1.065, 0.073*	*-2.9, 0.2, 2675*	Shaving the collimator's inboard aperture
5	Bremsstrahlung collimator	*1.278, -0.112*	*3.4, -0.3, 2675*	Shaving the collimator's outboard aperture
6	Missteer mask	*1.032, 0*	*3, 0, 2867*	Shaving the mask outboard aperture when both mirror and white beam stopper are out of position
7	Missteer mask	*-0.916, 0*	*-2.6, 0, 2873*	Shaving the mask inboard aperture
8	Gas Bremsstrahlung Stop	*-0.941, 0*	*-3.5, 0, 3718*	Direct impact on the Gas Bremsstrahlung stop

Source: Brookhaven National Laboratory

4.2.1. Results

The ambient dose equivalent rates resulting from GB irradiation in a normal operation scenario are detailed in Figure 4.3 for ARI and SXN. In Figure 4.4, the photon, electrons (and positrons) and neutron contributions are detailed. Dosimetry results outside of the shielding are shown in Table 4.2. The GB full power is distributed evenly between the two beamlines.

Regarding the ambient dose equivalent rates resulting from the maximum credible incidents detailed in Table 4.1, these are compiled in Table 4.3. Full GB power was assumed on all scenarios. The statistical uncertainty in the dose maps was lower than 8% at 30 cm from the shielding in the hotspots' vicinity.

Figure 4.3. Ambient dose equivalent rates in mrem/h resulting from GB impinging in scattering mirrors during normal ARI and SXN operation. The GB power load is distributed evenly between beamlines. In the top and middle panel, the results are averaged over Y=±4 cm whereas in the bottom they are averaged over 1 cm.

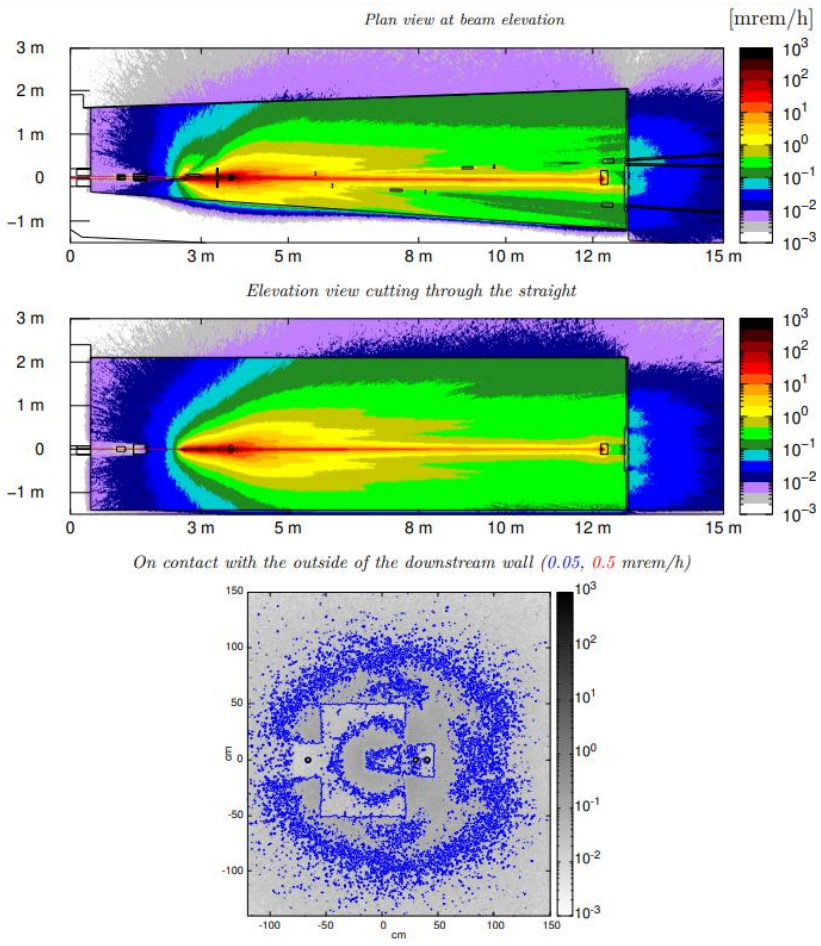

Source: Brookhaven National Laboratory

Table 4.2. Dosimetry analysis outside of the FOE shielding accounting for the GB during normal ARI and SXN operation

Max H*(10) in mrem/h due to neutron, gamma, beta radiation and overall maximum outside of the:						
	Outboard wall		Roof		Downstream wall	
	Contact	30 cm	Contact	30 cm	Contact	30 cm
n, γ, β±	*.014, .007, .020*	*.011, .004, .009*	*.015, .007, .020*	*.013, .006, .016*	*.078, .066, .236*	*.035, .050, .179*
Overall	*.028*	*.018*	*.030*	*.026*	*.340*	*.247*

Source: Brookhaven National Laboratory

4.2.2. Discussion

Based on the results shown in Figure 4.3, and compiled in Table 4.2, overall dose rates are lower than 0.05 mrem/h (0.5 μSv h^{-1}) on contact with the top of the roof and the outboard wall, meeting the design goals. Just outside of the downstream wall the dose rate values are

a factor of 5 higher than the design goal. The radiation levels outside of these shielding structures result from a combination of both electromagnetic and neutron radiation.

Figure 4.4. Plan (left) and elevation views (right) of neutron, electrons and photon ambient dose equivalent rates resulting from GB impinging in scattering mirrors during normal ARI and SXN operation. The GB power load is distributed evenly between beamlines. The results are averaged over Y=±4 cm and normalized to mrem/h.

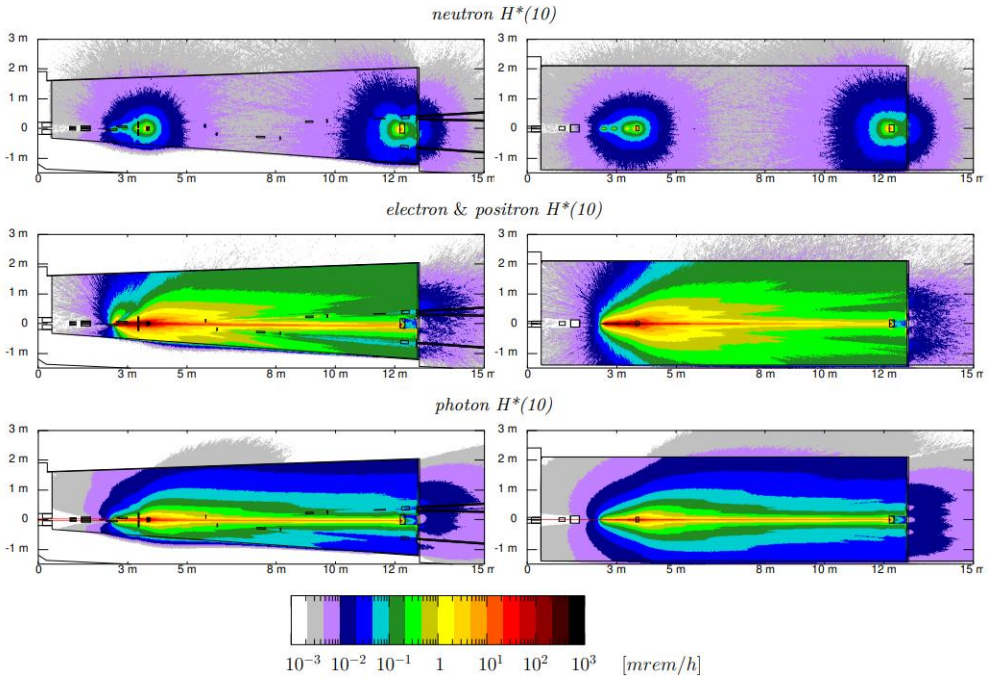

Source: Brookhaven National Laboratory

Table 4.3. Dosimetry results outside of the FOE shielding for the maximum credible incidents listed in Table 4.1.

Max H*(10) in mrem/h due to neutron, gamma, beta radiation (n, γ, β±) and overall maximum below, outside of the:						
Case	Outboard wall		Roof		Downstream wall	
	Contact	30 cm	Contact	30 cm	Contact	30 cm
1	*.022, .005, .004 .024*	*.015, .004, .004 .018*	*.015, .004, .004 .017*	*.009, .004, .004 .014*	*.001, .000, .000 .001*	*.001, .000, .000 .001*
2	*.036, .005, .003 .040*	*.026, .004, 003 .029*	*.017, .001, .005 .018*	*.012, .001, .001 .013*	*.002, .002, .004 .009*	*.001, .001, .003 .005*
3	*.030, .004, .002 .032*	*.020, .003, .002 .023*	*.013, .003, .004 .013*	*.010, .002, .003 .010*	*.033, .064, .050 .144*	*.007, .012, .022 .036*
4	*.006, .004, .004 .010*	*.005, .003, .003 .009*	*.007, .007, .008 .016*	*.005, .006, .007 .015*	*.032, .080, .217 .300*	*.020, .042, .138 .194*
5	*.008, .008, .006 .019*	*.006, .005, .005 .014*	*.006, .010, .010 .022*	*.004, .008, .009 .017*	*.043, .120, .185 .350*	*.019, .070, .088 .173*
6	*.008, .005, .005 .016*	*.007, .004, .004 .014*	*.008, .007, .009 .025*	*.007, .006, .007 .020*	*.110, .230, .729 1.090*	*.046, .171, .560 .770*
7	*.017, .001, .001 .018*	*.013, .000, .001 .014*	*.018, .001, .001 .018*	*.014, .001, .001 .015*	*.124, .005, .005 .130*	*.053, .002, .004 .056*
8	*.018, .001, .001 .019*	*.013, .001, .001 .014*	*.018, .001, .001 .019*	*.014, .001, .001 .015*	*.123, .004, .002 .128*	*.053, .002, .001 .054*

Source: Brookhaven National Laboratory

The electromagnetic component is mostly forward projected, cascading from the scattering mirrors and propagating throughout the beam line, interacting with its components.

Conversely, the neutron component is largely driven by two foci, consisting of the main interaction points of the GB with metals, namely the mask downstream of M1 mirror and the GB stop.

For the normal ARI-SXN operation, although the radiation levels on the downstream wall of the FOE still meet the radiological requirements of 0.5 mrem/h, they exceed the design goals and therefore the shielding configuration will need to be improved in future design iterations.

Possible solutions might involve the GB stop moving upstream or changing its shape/length, to mitigate the effect of neutron shine and protect the downstream wall more effectively from the electromagnetic cascade. Such modifications will be carefully planned to avoid interference with the beam line components and supporting structures.

The use of a hydrogenated material in tandem with the lead panel reinforcing the downstream wall is another option under consideration for neutron attenuation. Also, a lead layer covering the upstream section of the transport pipes will help to improve the shielding performance at the pipe/FOE wall interface.

The maximum credible incidents results compiled in Table 4.3 showed that the outboard walls and roof were adequately shielded in all cases considered.

In cases 3-5, the radiation level downstream of the FOE wall exceeded the design goals. The magnitude of the leakage is comparable to what was previously observed in the normal operation scenario. In these cases, the leakage is mainly driven by the electromagnetic cascade, hence minor lead based shielding improvements will likely suffice to attenuate radiation to acceptable levels. For cases 7 and 8, ambient dose equivalent rate values over 0.05 mrem/h (0.5 μSv h^{-1}) were found downstream of the FOE wall. In these last two cases

the radiation outside of shielding is driven by a strong neutronic component originating in the GB stop. A longer stop design would further improve these results. The worst-case scenario for the downstream wall was case 6, slightly exceeding 1 mrem/h (10 µSv h^{-1}) on contact. Although neutrons contribute considerably for that result, it is dominated by the electromagnetic cascade by over 90%.

Case 6 results differ quite significantly from case 7 because the panel extends between the two guillotines and the outboard guillotine is closer to the centreline (see Figure 4.2). This asymmetry leaves the SXN openings more exposed to leakage through the pipe but also the wall, both above and below the guillotine. The panel design will be extended up to the outboard limit of the guillotine and the lead cover around the transport pipe will also improve the results considerably.

4.3. Synchrotron Radiation

In the ARI-SXN beam line, SR is generated by two undulators at the 29-ID chamber with the characteristics detailed in Table 4.4 for 3 GeV and 500 mA operation. The longer period undulator will be installed downstream.

The SR entering the FOE will be, at maximum, 7.9 kW for ARI and 5.2 kW for SXN (in linear mode, see Table 4.5). However, in normal operation the power incident will be significantly lower.

Table 4.4. ARI and SXN 29-ID EPU parameters in linear mode

Parameter	Beamline	
	ARI	SXN
Length [m]	*2*	*2*
Period [m]	*0.070*	*0.050*
Peak magnetic field [T]	*1.149*	*0.981*
Undulator parameter K_{eff}	*7.70*	*4.63*
Horizontal fan angle [mrad]	*1.68*	*1.15*
Vertical fan angle [mrad]	*0.73*	*0.71*
Maximum power [kW]	*7.880*	*5.205*

Source: Brookhaven National Laboratory

For the SR shielding assessment, it was assumed that the GB radiation has been completely suppressed in the FOE, thus only the SR sources will be considered. The SR spectra was calculated with the analytical code STAC8 (Asano and Sasamoto, 1994) up to 200 keV, and its trend was compared with SRW data (O. Chubar and P. Elleaume, 1998), as denoted in Figure 4.5. STAC8 and SRW differ by a factor of ~2-3 as the aperture effect was factored into the SRW and not in the STAC8 calculation. This "uncorrected" STAC8 spectra will be employed in the white and pink beam dosimetry calculations as a built-in safety factor.

Figure 4.5. The EPU70 and EPU50 SR source spectra, generated via STAC8 (points) and the SRW data (lines).

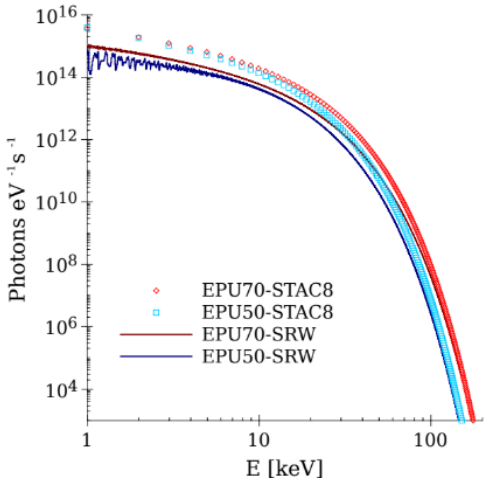

Source: Brookhaven National Laboratory

Since ARI-SXN beamlines are designed so that only the monochromatic beam exits the FOE the following conservative scenarios were considered:

1. Assessment of radiation leakage from the FOE due to SR

The STAC8 source term depicted in Figure 4.5 was modelled in FLUKA to assess the shielding performance of the FOE with both beamlines operating. ARI and SXN SR spectra were normalized to the maximum power delivered as per Table 4.4 and directed towards their respective M1 mirrors.

Radiation leakage underneath the FOE was assessed assuming a bare beam line (except for the M1 scattering mirrors) and, to facilitate statistic convergence, FOE walls were subdivided into 1–mm–thick biased layers. The geometry model of the FOE featured a shine blocker solution, with a 1 cm thick Pb panel extending 15 cm inwards along the concrete at the interface between the FOE wall and the structural concrete.

2. White beam impinging onto an optimum Si target and scattering towards the FOE's roof or outboard wall

The white beam scattering was modeled with STAC8 assuming either the ARI or SXN SR sources' striking a scatterer Si mirror at the M1 location upstream of the white beam stop. Since the mirrors are located approximately 1.67 m from the lateral wall and 2.1 m from the roof, the highest dose value throughout the total angular distribution was then calculated at those distances. Note that while the build-up factor was considered in the calculation, the SR polarization effect was not.

3. Scattered white beam striking the downstream wall at the interface between the FOE and the transport pipe

While the FOE downstream wall is nominally 5 cm thick and made of Pb, the inner side of the downstream wall is protected by the guillotine near the beam openings. The beam transport pipes consist of 3.8 cm diameter stainless steel pipes, 6 mm thick. If extra shielding is required, a layer of Pb can be added in some sections of the pipe. It will be hereby conservatively assumed that the minimum shielding thickness corresponds to 6 mm.

STAC8 was used to assess the radiological impact through a shielding element perpendicular to the beam. The mirror configuration was kept consistent with respect to the previous case, but with a 10 m distance between the scatter mirror and the downstream wall.

4. Pink beam is incident on a beam stopper in the upstream section of the beam transport pipe

The shielding necessary for a pink beam stopper to attenuate the beam was specified assuming, conservatively, that the pink beam could exit the FOE at the upstream end of the transport pipe.

Regarding the pink beam definition in STAC8, for ARI, it was considered an Au coated M1 mirror at 2° grazing angle, followed by a pair of zero order mirrors, with the same coating. The SXN case featured the M1 mirror, at 1.125° grazing angle, an M2 mirror pair, and the M3 mirror as well since SXN branches out still inside the FOE. As in ARI, M2 consisted of two zero order mirrors. As for M3, it was considered at 1.125° grazing angle similarly to SXN's M1. All SXN mirrors were Rh coated.

5: Monochromatic beam with highest specified operational energy, including higher harmonics, directed towards the pipe/vacuum chamber.

Ideally the beam is monochromatized inside the FOE and thus the pipe needs "only" to be monochromatic beam compatible throughout most of its extension.

As a worst-case scenario, it was considered that the monochromatic beam impinges directly onto the pipe or vacuum chamber, both 6 mm thick at minimum.

The monochromatic beam simulation featured the fundamental energies – 1 and 2.5 keV for ARI and SXN, respectively – and up to 10 harmonics. The fundamental fluxes considered were the maximum values at their respective samples. Thus, ARI's flux for its fundamental energy started at 10^{12} photons s^{-1} and SXN at 10^{11} photons s^{-1}, as shown in Figure 4.6.

Figure 4.6. Monochromatic beam source for ARI and SXN, obtained with STAC8 and normalized to the maximum fluxes at the sample. The integrated flux for ARI is 6.1×10^{12} photons s^{-1} and for SXN 2.2×10^{11} photons s^{-1}.

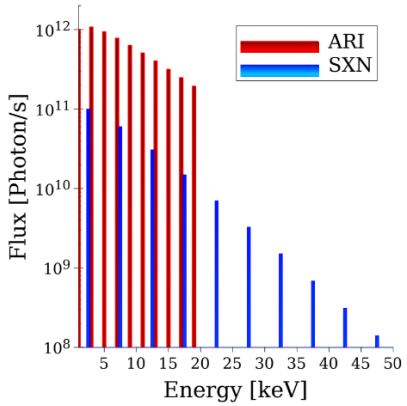

Source: Brookhaven National Laboratory

4.3.1. Results

H*(10) estimated with FLUKA is depicted in Figure 4.7, featuring a shine blocker solution. ARI and SXN outputs are combined, assuming maximum power of the SR as per Table

4.4. The statistical error of the maximum values is less than 10% on contact with the outside shielding walls.

The FOE shielding impact assessment of scattered SR is depicted in figures 8 and 9. Furthermore, the effect on the SR due to the successive interaction with mirrors and shielding was calculated with STAC8 and is displayed in Figure 4.10.

Dose rates due to SR, outside of the shielding, are listed in Table 4.5. An analysis of the radiological impact of the monochromatic beams, previously defined in Figure 4.6, is shown in Figure 4.11.

Figure 4.7. H*(10) FLUKA results, in mrem/h. The right panel depicts the plan view of radiation distribution near the ground level while the left panel corresponds is an elevation view averaged over 1 m approximately at the access door location.

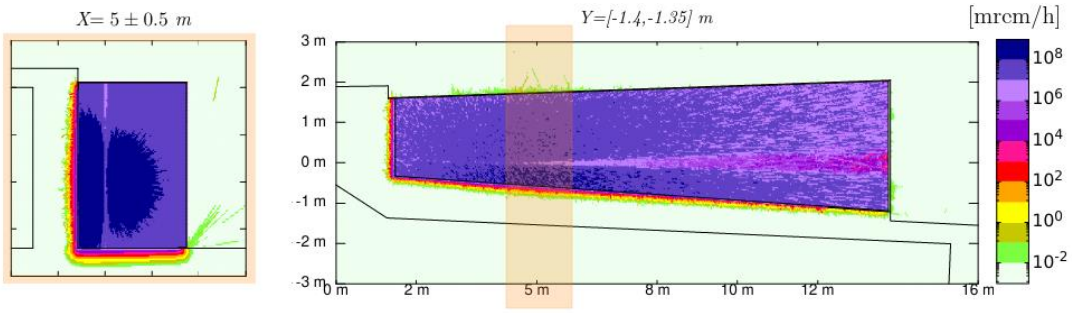

Source: Brookhaven National Laboratory

Figure 4.8. Angular distribution of the ambient dose rates (in mrem/h) outside of the roof (right panel) and lateral wall (left panel) computed with STAC8. ARI and SXN SR sources impinged onto their respective scattering targets at different angles and thus a range between the maximum and minimum values is provided. The points in the roof case denote FLUKA results.

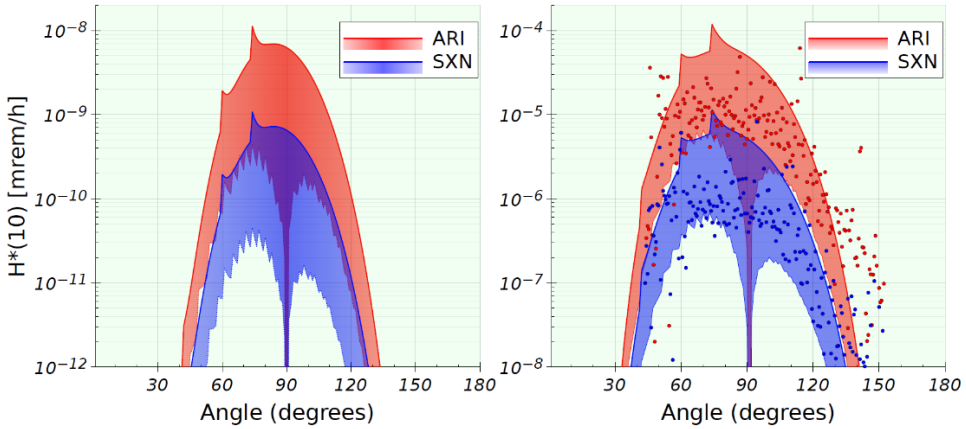

Source: Brookhaven National Laboratory

Figure 4.9. Angular distribution of the forward projected component of scattered radiation, computed with STAC8, in units of mrem/h. The radiation results from ARI and SXN SR sources scattering off their respective targets at 10 m from Pb and or Fe shielding walls with thicknesses ranging from 1–2 cm.

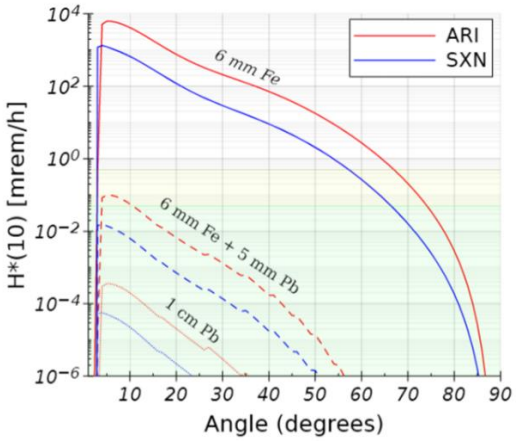

Source: Brookhaven National Laboratory

Figure 4.10. ARI and SXN photon spectra resulting from the sequential interaction of the beam with various mirrors and shielding elements, computed with STAC8.

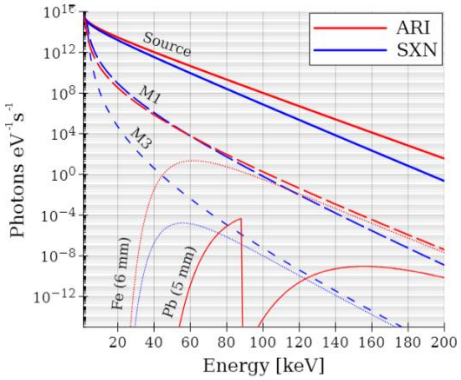

Note: Only the non-zero order mirrors were accounted for, and, for ARI, two consecutive shielding barriers were considered (6 mm Fe and 5 mm Pb) whereas for SXN only a 6 mm Fe barrier was used. The effect of the K-edge for Pb (at approximately 88 keV) is clearly visible in the ARI case.
Source: Brookhaven National Laboratory

Table 4.5. H*(10) [mrem/h] results obtained for various ARI-SXN SR scenarios.

ARI	Shielding				Maximum H*(10) [mrem/h]	
Scenario	location	material	Thickness [mm]	Distance [m]	contact	At 30 cm
Direct white beam	FOE downstream wall	Pb	50	-	0.0	0.0
Scattered white beam	FOE roof	Pb	10	2.1	4.3×10^{-5}	3.3×10^{-5}
Scattered white beam	FOE outboard wall	Pb	18	1.7	4.3×10^{-9}	3.2×10^{-9}
Scattered white beam	FOE/transport pipe interface	Fe+Pb	6+5	10	0.12	0.11
Pink beam	FOE/transport pipe interface	Fe+Pb	6+5	-	3.1×10^{-4}	3.0×10^{-4}
Pink beam	Beam stopper	Fe	30	-	0.05	0.05
Monochromatic beam	Transport pipe/ vacuum chamber	Fe	6	-	0.0	0.0
SXN	Shielding				Maximum H*(10) [mrem/h]	
Scenario	location	material	Thickness [mm]	Distance [m]	contact	At 30 cm
Direct white beam	FOE downstream wall	Pb	50	-	0.0	0.0
Scattered white beam	FOE roof	Pb	10	2.1	4.0×10^{-6}	3.0×10^{-6}
Scattered white beam	FOE outboard wall	Pb	18	1.7	4.0×10^{-10}	2.8×10^{-10}
Scattered white beam	FOE/transport pipe interface	Fe+Pb	6+5	10	1.8×10^{-2}	1.7×10^{-2}
Pink beam	FOE/transport pipe interface	Fe	6	-	2.5×10^{-5}	2.5×10^{-5}
Monochromatic beam	Transport pipe/ vacuum chamber	Fe	6	-	0.67	0.56

Note: All White and pink beam cases calculated with STAC8 while the monochromatic beam cases were calculated with FLUKA
Source: Brookhaven National Laboratory

Figure 4.11. H*(10) [mrem/h] resulting from the direct impact of the ARI (right panel) and SXN (left panel) monochromatic beam through a 6 mm Fe barrier.

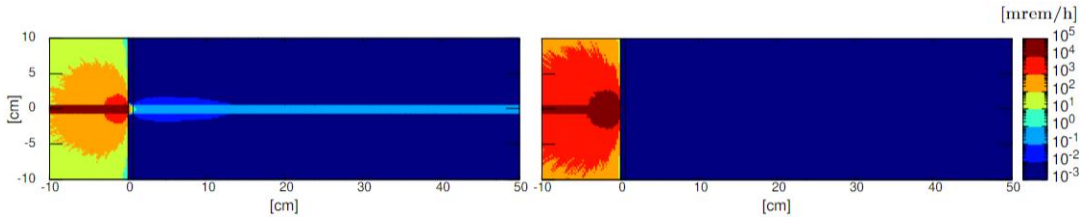

Source: Brookhaven National Laboratory

4.3.2. Discussion

Ambient dose equivalent rates were found to be lower than 0.05 mrem/h (0.5 μSv h^{-1}) outside of the FOE when lead shine blockers 1 cm thick and 15 cm long are employed at the interface between the hutch wall and concrete (see Figure 4.7).

Regarding the shielding effectiveness of the downstream wall against SR radiation, it was found that even a direct impact of the SR sources shown in Figure 4.5 would not pose a radiological concern as the radiation levels outside of the downstream wall were lower than background – see Table 4.5.

The white beam scattering results were lower than 0.05 mrem/h (0.5 μSv h-1) outside of the roof and lateral wall for both ARI and SXN, as denoted in Figure 4.8 and Table 4.5. The fields were higher above the roof due to thinner shielding and the FLUKA values generated were in relatively good agreement with the STAC8 results.

On the other hand, as it was assumed that the interface between the downstream wall and the pipes could have as low as 6 mm of iron thickness, there was potential for substantial radiation leakage further downstream as shown in Figure 4.9. Nevertheless, this forward projected component of the white beam scattering could be adequately shielded if a layer of at least 5 mm of lead is applied to the beam transport pipe. Such solution would likely be required along some length of the upstream section of the beam transport pipe only, the exact length will be defined according to the raytracing information.

Additional scattered white beam results can be found in Table 4.5. The results for ARI exceed the design goal by at least a factor of 2 but one should note that it corresponds to both the maximum from the angular distribution and a direct incidence on the shielding.

As for the pink beam cases studied, even using conservative assumptions for the M2 mirrors, the results obtained are well below background for both ARI and SXN for the FOE/pipe interface scenario (see Table 4.5). Since the SXN has one more mirror than ARI before exiting the downstream wall, its shielding impact is lower than in the ARI case, this can be visualized in the photon spectra shown in Figure 4.10. In fact, SXN pink beam can be directly stopped with the pipe thickness only, whereas ARI necessitates a lead layer around the transport pipe for an effective shielding. Further downstream, the ARI pink beam can be radiologically stopped with a 3 cm Fe beam stopper.

Monochromatic beam results were estimated with FLUKA considering the beams' direct impact onto the nominal transport pipe thickness or vacuum chamber (6 mm of iron). Although SXN featured a factor ~ 10 less photon flux than ARI's, the former higher fundamental energy of 2.5 keV (and its harmonics) made it more challenging to shield radiologically. This effect is illustrated in Figure 4.11, showing that the 6 mm Fe thickness is barely able to shield the SXN monochromatic beam but suffices in the ARI case. Adding 1 mm of iron to the transport pipe would meet the design goals for SXN (the TVL derived from the FLUKA result is 0.85 mm). However, the SXN monochromatic result is largely driven by the last 3 harmonics. Thus, if one accepts 7 harmonics to be a reasonably conservative assumption then the SXN results are ~5×10^{-4} mrem/h (calculated with STAC8) and thus meet the design goal.

4.4. Summary and Conclusions

This study consisted of a preliminary shielding analysis for the new NSLS-II 29-ID ARI and SXN beamlines. The preliminary results indicate that the shielding requirements specified in this document complies with the NSLS-II shielding policy.

The main findings in this work are summarized below:

- In the normal operation scenario, with GB beam directed to the M1 mirrors and the optimal GB beam stop and lead panel in place, the design goal of 0.05 mrem/h (0.5 μSv h^{-1}) can be achieved with minor shielding improvements that will be specified in future iterations.
- Maximum credible incidents exceed the radiological requirements in one of the eight configurations studied (case 6) downstream of the FOE. However, it is envisaged that minor shielding design modifications will mitigate the radiation leakage.
- No radiation leaks through the FOE walls are expected due to the SR scattering. Neither floor nor skyshine issues are anticipated if shine blockers are properly employed. Validation of the shine blocker dimensions with a more detailed FOE model will ensue in a forthcoming evaluation.
- The interface of the FOE wall with the beam transport pipe was singled out as a weak spot in the shielding for SR in this work. Since raytracings were not available, conservative assumptions were used for that interface, including scattered white beam. However, even with a minimal complement of 5 mm of lead to the transport pipe the results are relatively benign.
- Radiation leakage throughout the pipe and vacuum chamber were assessed assuming pink beam or monochromatic beam directly impacting the shielding. Preliminary findings indicate that the ARI pink beam is relatively more challenging to attenuate, requiring up to 5 cm lead wrap or a 3 cm Fe stopper. On the other hand, the SXN monochromatic beam is more difficult to stop radiologically than ARI's but, even with 7 harmonics employed in the SXN monochromatic beam source, the 6 mm of Fe are sufficient to meet the shielding design goals.

4.5. List of references

T. T. Bohlen et al., "The FLUKA Code: Developments and Challenges for High Energy and Medical Applications", *Nuclear Data Sheets* **120**, 211 (2014).

A. Ferrari, P. R. Sala, A. Fassò, and J. Ranft, "FLUKA: a multi-particle transport code" (2005), CERN-2005-10, INFN/TC_05/11, SLAC-R-773.

P. R. Sala et al., "The FLUKA group- and point-wise neutron treatment", these proceedings.

A. Ferrari et al., "FLUKA: status and perspectives", these proceedings.

A. Ferrari, M. Pelliccioni, and P. R. Sala, "Estimation of fluence rate and absorbed dose rate due to gas bremsstrahlung from electron storage rings", *Nuclear Instruments and Methods in Physics Research B* **83**, 518 (1993).

P. K. Sahani, G.Haridas, A. K. Sinha, K. V. A. N. P. S. Kumar, and T. A. Puntambekara, "Interaction of electrons with residual gas molecules and its effect on gas bremsstrahlung radiation in electron storage rings", *Radiation Physics and Chemistry* **156**, 252 (2019).

A. Marendziak, A. I. Wawrzyniak, M. Zajac, S. Piela, and M. J. Stankiewicz, "Residual gas in the vacuum system of the SOLARIS 1.5 GeV electron storage ring", in *Proceedings of IPAC2017* (2017).

V. Vlachoudis, "FLAIR: A Powerful but User Friendly Graphical Interface For FLUKA", in *Proc. Int. Conf. on Mathematics, Computational Methods & Reactor Physics (MC 2009)* (2009).

Y. Asano and N. Sasamoto, “Development of shielding design code for synchrotron radiation beam line”, *Radiation Physics and Chemistry* **44**(1-2), 133 (1994).

O. Chubar and P. Elleaume, “Accurate and Efficient Computation of Synchrotron Radiation in the Near Field Region”, *Proc. of EPAC-98,* 1177-1179 (1998)

4.6. List of abbreviations and acronyms

ALARA	As low as reasonably achievable
ARI	ARPES and RIXS Imaging
ARPES	angle-resolved photoemission spectroscopy
EPU	Elliptically polarizing undulator
FLUKA code	FLUktuierende KAskade MC particle transport and interaction
FOE	First Optical Enclosure
GB	Gas Bremsstrahlung
MC	Monte Carlo (method)
NEXT-II	National Synchrotron Light Source Experimental Tools Two
NSLS-II	National Synchrotron Light Source II
RIXS	resonant inelastic x-ray scattering
SR	Synchrotron Radiation
STAC8 code	High energy synchrotron radiation beamlines shielding design
SXN	Soft X-ray Nanoprobe Beamline

5. The skyshine problem at the STAR facility due to the beam dumps and the dark current leakage

Federico Chiarelli[1*], Adolfo Esposito [1], Raffaella Donghia [1], Maurizio Chiti [1], Daniele Chiti [1], Agostino Raco [1]
[1]Istituto Nazionale di Fisica Nucleare (INFN-LNF)
[*]federico.chiarelli@lnf.infn.it

STAR (Southern Europe Thomson Back-Scattering Source for Applied Research) is an "inverse-Thomson scattering" facility based on the Calabria's University campus in Rende, Italy, it will be used for advanced scientific investigation on fundamental and applied materials research, with produced monochromatic Xrays [1,2].

The facility upgrade consists in two electron beam lines: the first one can accelerate electrons up to 150 MeV, and the second one up to 85 MeV. The Xrays are produced through electron beam-laser interaction, and they will be used in two experimental areas to perform investigation on biological, polymeric and composite materials as well as in the cultural heritage field.

In order to obtain the STAR license, several radiation protection studies have been performed through the Monte Carlo code FLUKA, and in particular the one related on the skyshine radiation. The importance related on this topic is due to the presence of this machine inside the university campus, as well as the presence of offices and other occupied areas.

The skyshine radiation problem has been assessed for:

- *the prompt radiation related to the beam dumps designed for each beam line;*
- *the prompt radiation due to the dark current leakage;*
- *the local shielding proposed for the same leakage.*

First, two different points have been considered for the ambient dose evaluation, both on the roof into directions of the areas of interest.

The FLUKA simulations performed, with different conservative approaches, highlithed the no radiological relevance due to the skyshine radiation. Indeed, trivial dose values have been obtained in the areas of interest, such as offices and parking.

5.1. Introduction

STAR (Southern Europe Thomson Back-Scattering Source for Applied Research) is an "inverse Thomson scattering" facility sited at the Calabria's University campus in Rende, Italy [1,2].

Its upgrade consists of two electron beam lines realization: the first one, at high energy, allows to accelerate electrons until 140 MeV, while the second one, at low energy, up to 85 MeV (Figure 5.1). At the end of these lines, monochromatic X-ray beams are produced through the electron beam-laser interaction, at 350 keV and 70 keV respectively for the high and low energy line. These will be used in two experimental areas to perform investigation on biological, polymeric and composite materials and in the cultural heritage field. In this work, the skyshine induced dose during normal working condition has been studied for three different cases: the radiation field produced in the beam-dump interaction; the dark current leakage along the beam lines; the radiation field produced from beam-dump interaction in the magnetic field absence condition, considered for the correct beam alignment and for the beam characteristics study. The need of this skyshine evaluation is due to the bunker's roof reduced thickness, which is around 50 cm, and the machine position inside a university campus, that means close to occupied areas like offices. The

aim is to ensure the no radiological relevance inside these places, reached through trivial doses, that correspond to a total annual dose equivalent value less than 10 µSv.

Figure 5.1. Schematic 3D layout of STAR facility

Schematic 3D layout of the STAR facility upgrade. The high energy beam line is on the left while the low energy one is on the right.

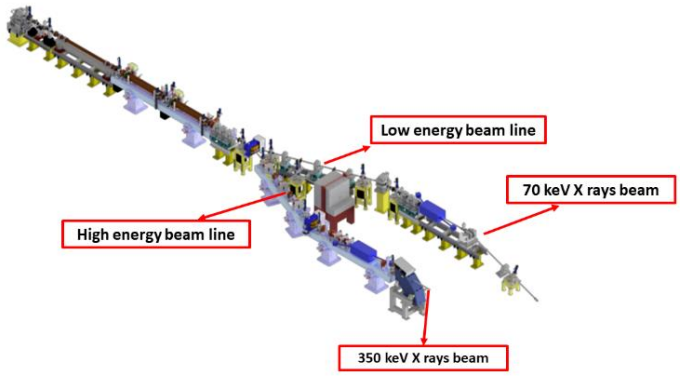

5.2. The skyshine evaluation

The skyshine evaluation means to quantify in the total ambient dose equivalent for the different cases previously introduced in two points placed on the roof, named A and B (Figure 5.2), directed to the areas of interest. These estimations have been performed through dedicated Monte Carlo simulations with FLUKA code, version 2021.2.5 [3,4,5,6].

The working parameters for the high and low energy cases are referred to the normal working conditions. For the dark current leakage cases, instead, the beam sizes, the effective energy and the deflection angle have been chosen through a dedicated simulation performed by A. Bacci and L. Faillace [8], reported in the Section 5.7. The high energy case and the related dark current leakage is analysed below, while the other cases are available in Sections 5.8-5.10. The beam parameters considered for these simulations have been reported in Table 5.1.

Figure 5.2. Position of the point A and B on the roof

This picture shows the position of points A and B used for the skyshine evaluation, reproduced through Flair [7]. Point A, on the left, is directed to the offices while the point B, on the right, is directed to the parking.

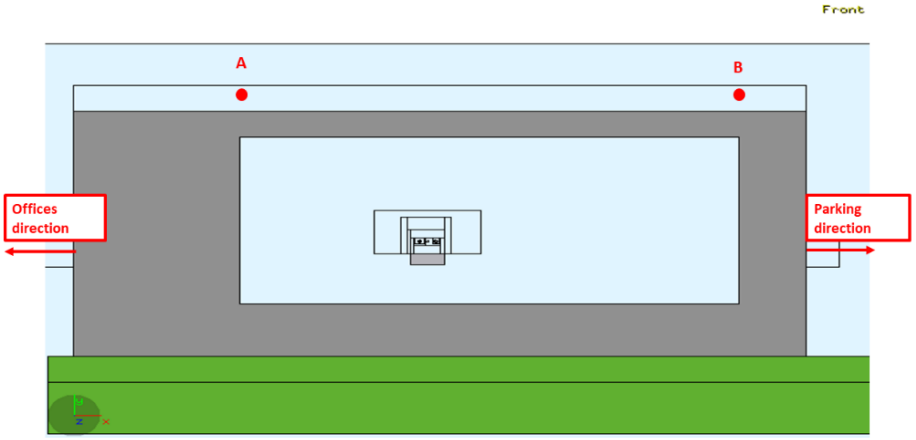

Table 5.1. Working parameter for the different cases studied

The table shows the working parameters considered for the simulations performed. For the high and low energy beam dump case, a pencil beam has been used. For these cases, the mean current is composed by 50 nA of beam current and 3 nA of dark current. For the dark current leakage and for diagnostic study cases, a dedicated simulation has been performed by A. Bacci and L. Faillace [8], available in Section 5.7.

	Mean current [nA]	Frequency [Hz]	Energy [MeV]	Beam surface [cm^2]
High energy beam current	53	100	140	$8 \cdot 10^{-4}$
Low energy beam current	53	100	85	$8 \cdot 10^{-4}$
High energy dark current leakage	3	100	125	0.13
Low energy dark current leakage	3	100	80	0.13
Diagnostic study (absence of magnetic field)	0.56	1	140	0.64

5.3. High energy beam current case

The skyshine evaluation for the high energy beam current case is related to the radiation field produced by electron beam-dump interaction, when STAR works in the high energy mode. The beam dump considered for the simulation has a cylindrical shape and it is located at 90 degrees into the floor, in order to simultaneously reduce the backscattering contribution and so to facilitate the X-ray line directed to the experimental hall (Fig. 5.3). The beam dump structure, reported in Fig. 5.4, has been used also for the low energy beam current case, described in Section 5.8. The total ambient dose equivalent distribution obtained from the simulation is reported in Figure 5.5 on the xz plane on the roof. The underlined areas in Figure 5.5 represent the areas characterized by the highest total dose equivalent values, thus useful for the skyshine estimation. In order to pursue a conservative approach, only the highest dose value has been considered from these areas, they are 0.4 µSv/h for point A, directed to the offices, and 0.35 µSv/h for point B, directed to the parking.

Figure 5.3. A schematic 2D projection for the high energy case

This picture shows the geometrical layout for the high energy case. For this case, the beam dumo is placed perpendicularly into the floor, to reduce the backscattering contribution and to facilitate the X-ray line.

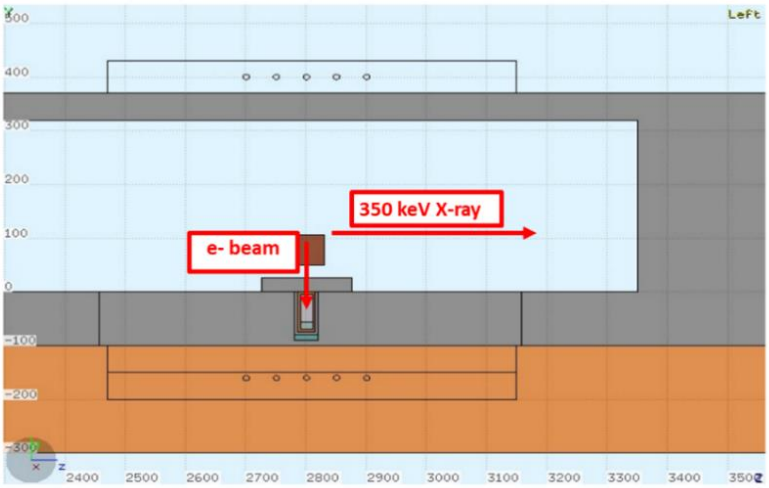

Figure 5.4. The beam dump structure

This picture shows the beam dump structure considered for the high and low energy working conditions. It is composed by: an aluminium core, used for the complete electromagnetic shower development, a tungsten layer placed after the core, used for the forward spike attenuation, a copper cover useful for the heating transmission, a lead cover for photon attenuation and a polyethylene layer, at the end of the structure, used for neutron attenuation.

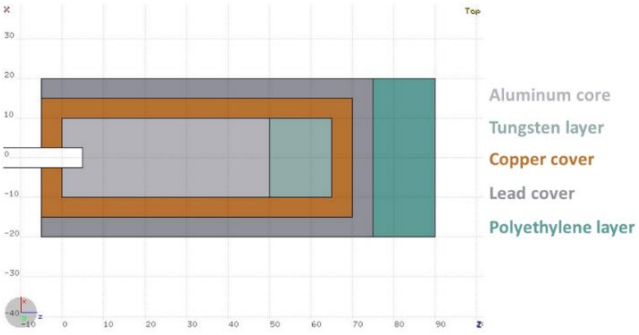

Figure 5.5. Total ambient dose equivalent distribution on the roof

The figure shows the total ambient dose equivalent distribution on the roof for the high energy beam current case.

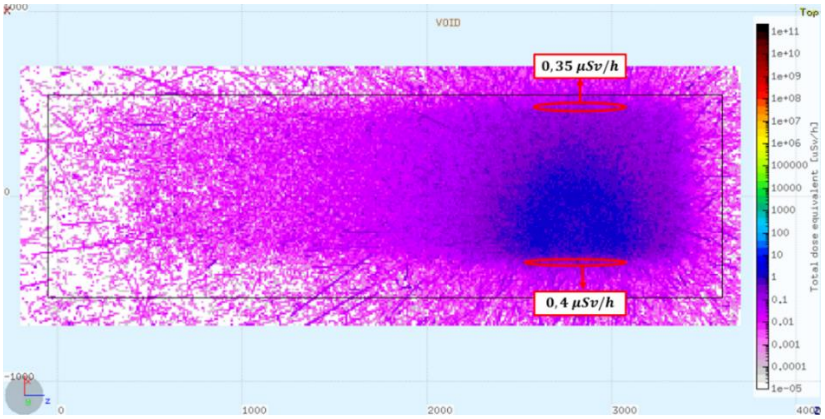

5.4. Dark current leakage along the high energy beam line

The skyshine evaluation related to the dark current leakage has been estimated for two different cases, along the high energy and low energy beam line, referred to the different working conditions [9,10]. The leakage along the high energy beam line is reported and discussed here, while the low energy case are available in the Section 5.9.

In order to perform a simulation as realistic as possible, the geometrical layout close to the dipole has been rebuilt through CAD information (Figure 5.6 (a)). For the irradiation conditions reported in Table 5.1, the total dose equivalent beyond the roof are high enough, exceeding the trivial dose, thus a local shielding for each case has been considered. This shielding near the point source is composed by a first lead layer, placed close the beam pipe, and an upper polyethylene cover, used to intercept and attenuate the neutron contribution direct on the roof (Figure 5.6 (b)). The irradiation conditions for the dark current leakage along the high energy beam line are reported in Table 5.1. The total ambient dose equivalent distribution on the roof obtained for this case is reported in Figure 5.8. The underlined zones in Figure 5.7 represent the critical areas on the roof characterized by the highest dose equivalent values. In order to pursue a conservative approach, only the highest dose values have been considered from these areas, and they are 1.7 µSv/h for the point A and 0.6 µSv/h for the point B.

Figure 5.6. 3D layout STAR close to the dipole

The figure on the left shows a 3D projection of the STAR facility near the magnetic dipole, while the figure on the right shows the local shielding proposed and considered for the dark current leakage along the high energy beam line.

(a) (b)

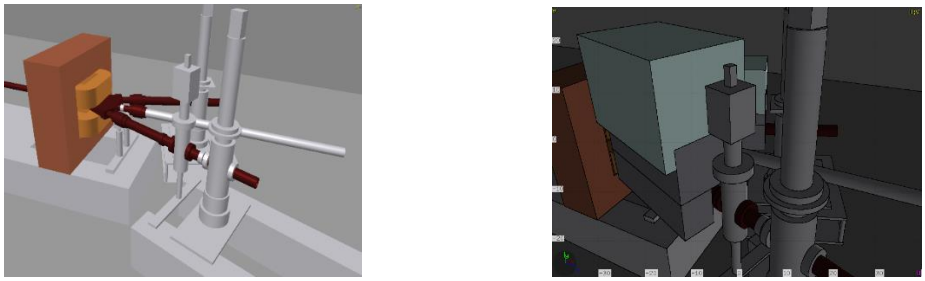

Figure 5.7. Total ambient dose equivalent on the roof

The figure shows the total ambient dose equivalent distribution for the dark current leakage during the high energy mode.

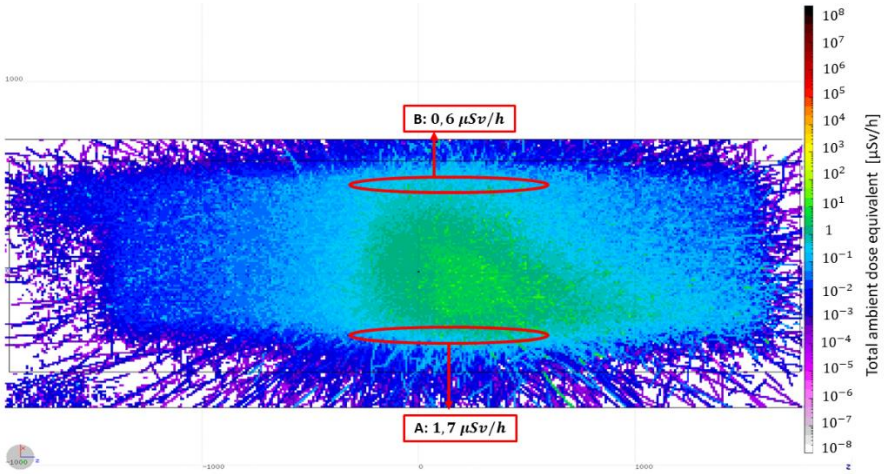

5.5. Summary and Conclusions

The skyshine problem has been analysed for three cases: the first one considers contribution related to the electron beam-dump interaction and the related dark current leakage when STAR works in high energy mode; the second one is analogue but referred to the low energy working mode; the third case represents the diagnostic study in absence of magnetic field and at 0 degrees from the dipole. Considering a total working time of 6000 hours per year, 3000 for each working mode, it is possible to estimate the annual dose equivalent at point A and B on the roof. These evaluations have been summarized in Table 5.2. In order to be conservative, the dose values reported in Table 5.2 have been considered as source points direct on the places of interest. In the related occupied areas, the annual dose equivalent has been estimated through the inverse square law, neglecting every attenuation

contribution between the source points and the places of interest, such as hangar wall, air attenuation or the presence of other absorbing media. The distance from the bunker are 23 m for the offices and 33 m for the parking. The results obtained with this approach are summarized in Table 5.3. It is possible to note that, although a conservative approach has been used, the total dose equivalent values obtained into the places of interest result lower than the trivial values, 10 µSv per year, in every possible working condition.

Table 5.2. Total annual ambient dose equivalent on the roof

The table shows the annual ambient dose equivalent values at points A and B in the different working conditions. The values have to be considered as the sum of the dose value for the high/low energy beam and the dark current leakage related to it. The last irradiation condition is referred to the diagnostic study and the alignment at 0 degrees.

Irradiation condition	A [mSv/y]	B [mSv/y]
High energy beam current + dark current leakage	6.3	2.9
Low energy beam current + dark current leakage	2.7	4.7
Diagnostic study (absence of magnetic field)	1.9	1.0

Table 5.3. Total annual ambient dose equivalent at the place of interest

The table reports the annual ambient dose equivalent in the places of interest for every possible working conditions.

Irradiation condition	Dose at office area [µSv/y]	Dose at parking area [µSv/y]
High energy beam current + dark current leakage	9.7	2.0
Low energy beam current + dark current leakage	4.1	4.1
Diagnostic study (absence of magnetic field)	2.9	1.0

5.6. List of references

[1] A. Bacci, L. Faillace et al (2021), "*STAR HE-linac Complete detailed Design Report*".

[2] https://star.unical.it/ .

[3] T.T. Böhlen et al, "*The FLUKA Code: Developments and Challenges for High Energy and Medical Applications*", Nuclear Data Sheets 120, 211-214, 2014.

[4] A. Ferrari et al, "FLUKA: a multi-particle transport code", CERN-2005-10, INFN/TC_05/11, SLAC-R-773, 2005.

[5] Ferrari, A. et al., "FLUKA: status and perspectives", these proceedings.

[6] Sala P. et al., "The FLUKA group- and point-wise neutron treatment", these proceedings.

[7] Vlachoudis V., "Flair: a powerful but user friendly graphical interface for FLUKA", Proc. Int. Conf. on Math, Computational Methods & Reactor Physics (M&C 2009), Saratoga Springs, New York, 2009.

[8] Private communication by A. Bacci and L. Faillace.

[9] D. Alesini et al, "*The new SPARC_LAB RF photo-injector*", 13th Int. Particle Acc. Conf. IPAC2022, Bangkok, Thailand, JACoW Publishing, ISBN: 978-3-95450-227-1, ISSN: 2673-5490, doi: 10.18429/JACoW-IPAC2022-MOPOMS019, pp. 671-674.

[10] N.V. Mokhov et al, "*Dark current and radiation shielding studies for the ILC main LINAC*", Fermilab-Conf-16-542-APC-TD, December 2016.

5.7. Annex A: Dark current analysis

The dark current analysis has been performed through a dedicated simulation by A. Bacci and L. Faillace [6] for the high energy case. This analysis has been centered on the investigation of the energy distribution spectra and the deflection of the dark current from the bending magnet. Two detectors have been considered, appointed as Screen 1 and Screen 2, and placed respectively before and after the dipole (Figure 5.A.1).

The results obtained from these screens are reported in the Figure 5.A.2. These have been useful to define the beam size before the magnet, for the diagnostic study case, and after it for the leakage along the beam lines, respectively from Figure 5.A.2 (a) and Figure 5.A.2 (b) respectively. Furthermore, Figure 5.A.2 (c) has been used to define the effective energy for these last cases. The deflection angles have been calculated from the knowledge of the beam pipe, its position in the layout, and from the spatial dispersion reported in Figure 5.A.2 (b). The maximum deflection angle has been considered in the FLUKA simulation in order to obtain a point source as far as possible from the dipole, Figure 5.A.2 (d). Although the measured current in the same gun of STAR is around 2.2 nA, a value of 6 nA has been considered, into the simulations performed, in order to introduce a safety factor. After the dipole a percentage around 50 % is lost into the beam pipe, Figure 5.A.3, it corresponds to the dark current leakage along the beam line, 3 nA, reported in Table 5.1

Figure 5.A.1 Schematic layout for the dark current analysis

The figure shows the schematic layout used for the dark current analysis, and the detector positions.

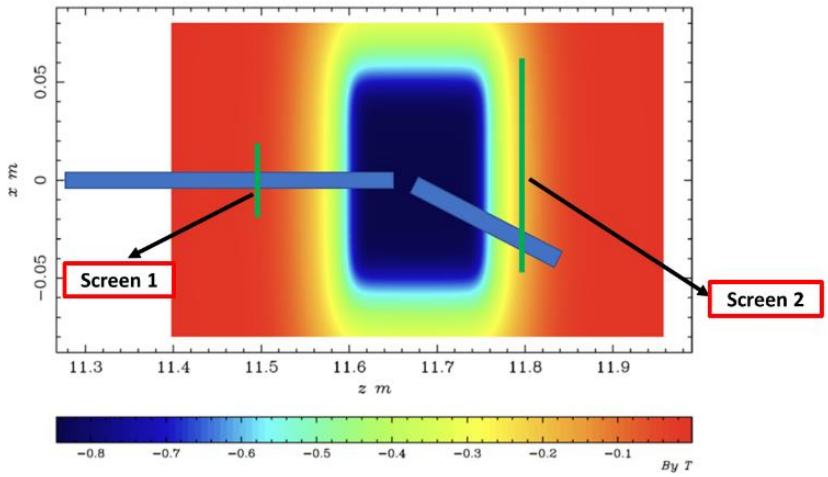

Figure 5.A.2. Results of the dark current analysis

The figure shows the results related to the dark current analysis, in terms of spatial distribution before (a) and after (b) the dipole, and the energy spectrum (c). The figure (d) represents the point source obtained with the maximum deflection angle along the beam line.

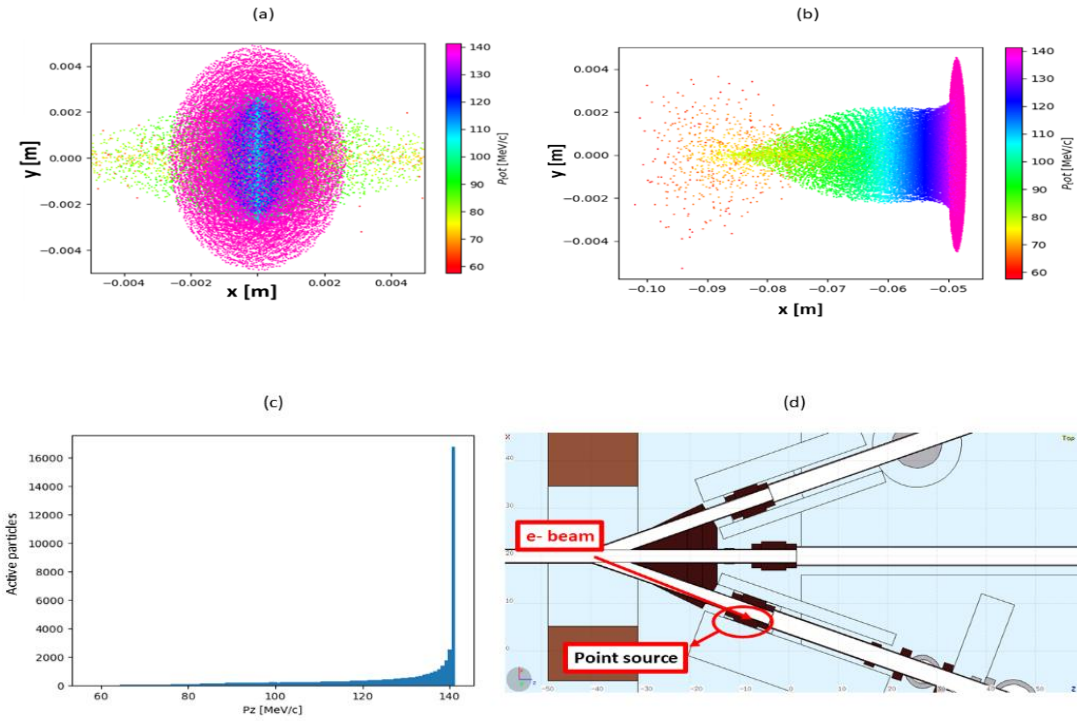

Figure 5.A.3. Dark current profile

The figure shows the dark current profile during the dipole crossing.

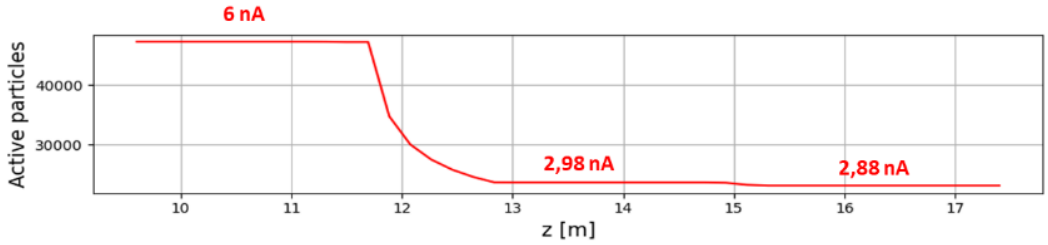

5.8. Annex B: FLUKA simulation for the low energy case

In the FLUKA simulation for the low energy case the same beam dump structure used for the high energy case, Figure 5.4, has been considered, but positioned at 20 degrees to the floor, as reported in Figure 5.B.1. The total ambient dose equivalent distribution on the roof obtained for this case is reported in Figure 5.B.2. As for the high energy case, the underlined

zones in Figure 5.B.2 represent the critical areas considered for the skyshine estimation. Only the highest dose values have been considered from these areas and they are 0.2 µSv/h for point A and 0.8 µSv/h for point B.

Figure 5.B.1. STAR layout for the low energy case

The figure shows the STAR layout considered for the low energy beam current case.

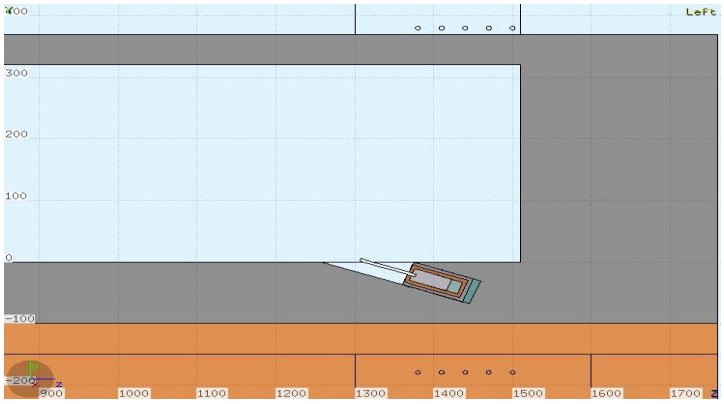

Figure 5.B.2. Total ambient dose equivalent on the roof for the low energy case

The figure shows the total ambient dose equivalent distribution on the roof for the low energy case.

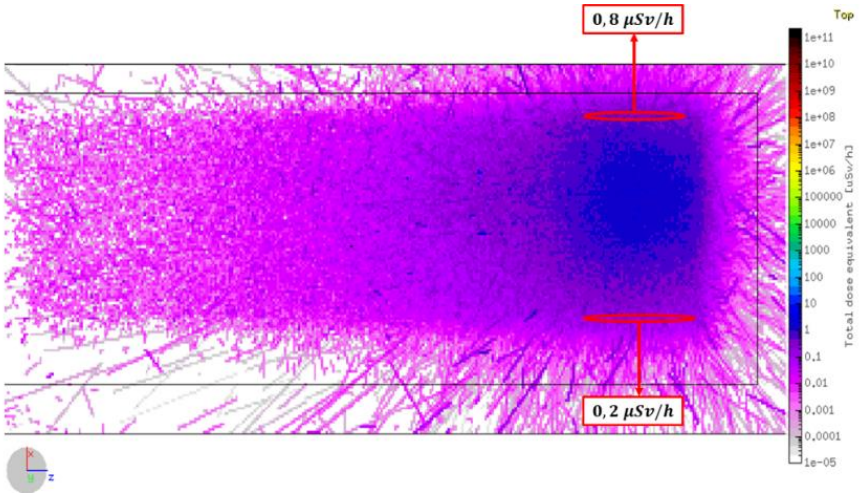

5.9. Annex C: FLUKA simulation for the dark current leakage for the low energy case

The local shielding proposed for the dark current leakage along the low energy beam line is very similar to that of the high energy and it is reported in Figure 5.C.1. The total ambient dose equivalent distribution obtained on the roof is reported in Figure 5.C.2.The underlined zones in Figure 5.C.2 represent the areas used for the skyshine estimation. As in the previous cases, only the highest dose values have been considered from these areas, and they are 0.7 µSv/h for point A and 0.8 µSv/h for point B.

Figure 5.C.1. 3D layout of the local shielding for the low energy beam line

The figure shows the 3D layout of the local shielding proposed for the low energy beam line. As for the high energy case, it is composed by a first lead layer close to the beam line, and an upper polyethylene cover.

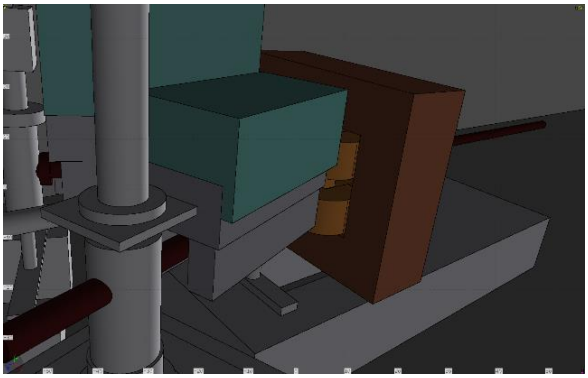

Figure 5.C.2. Total ambient dose equivalent on the roof for the dark current leakage along the low energy beam line

The figure shows the total ambient dose equivalent distribution on the roof for the dark current leakage related to the low energy working condition.

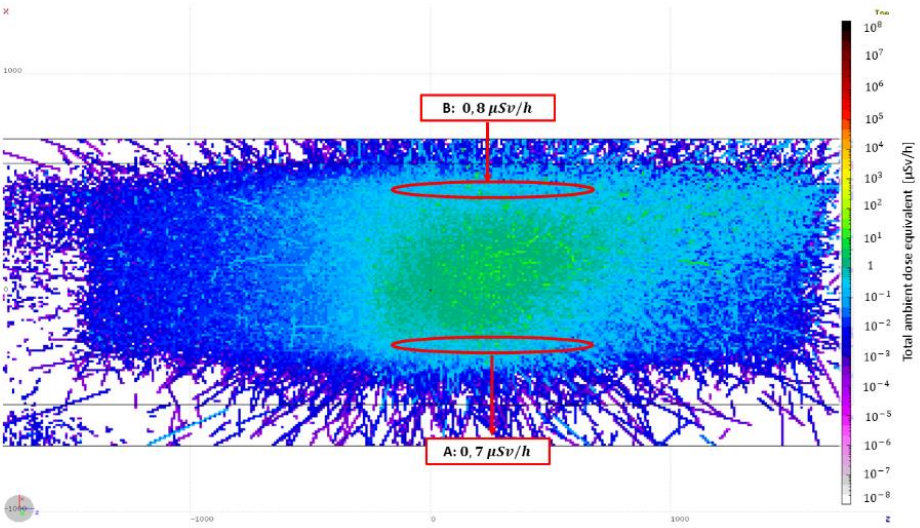

5.10. Annex D: FLUKA simulation for diagnostic study case

The FLUKA simulation for this case includes a beam dump placed in front of the dipole, used to reduce the photon and neutron contribution produced during the alignment and diagnostic study operations. This dump is composed of a lead block, upper covered by a polyethylene layer (Figure 5.D.1). The primary beam is composed of 140 MeV electron, with a frequency of 1 Hz and a mean current of 0.56 nA (0.5 nA of beam current and 0.06 nA of dark current) as reported in Table 5.1. It can be noted that this case considers a scaled frequency, from 100 to 1 Hz, and consequently a scaled mean current, because for

diagnostic operations the entire repetition frequency is not necessary. The ambient dose equivalent distribution on the roof obtained for this case is reported in Figure 5.D.2. As in the previous cases, only the highest dose values have been considered from the zones, and they are 0.6 µSv/h for point A and 0.4 µSv/h for point B.

Figure 5.D.1. 3D projection for the diagnostic beam dump

The figure shows the diagnostic beam dump proposed for this case.

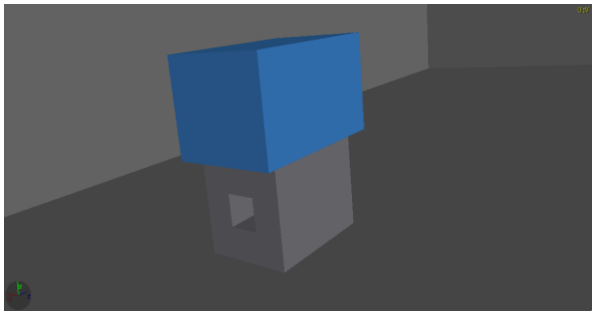

Figure 5.D.2. Ambient dose equivalent distribution for diagnostic study case

The figure shows the ambient dose equivalent distribution for the diagnostic study case.

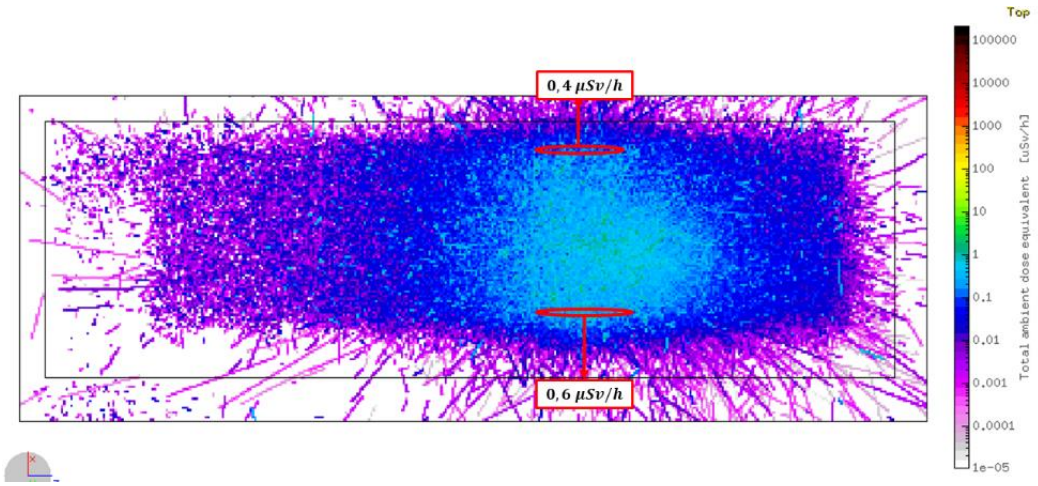

6. Fundamental investigation on concrete composite for radiation shielding in facilities

Ken-ichi Kimura[1], Nobuhiro SHIGYO[2], Nobuo Ikeda[2]
[1] Fujita Co.
[2] Kyusyu University
Corresponding Author(s): kkimura@fujita.co.jp

For the buildings where radiation exists, such as nuclear power plants or accelerator facilities, concrete is not only used as structural materials but also widely used as shielding materials. On the other hands, only few discussions had conducted for the constant of shielding calculation. In addition, very old and/or foreign data have been used for the calculation, such as ANL-5800 and JAERIM 6928, which had few information except for elemental composition. And some of the elemental fraction value are away from these of the actual concrete, typically Hydrogen. So major analyzed element data in various concrete samples used in actual facilities were presented, comparing the data in the past work, and were discussed referring the idea of concrete engineering. In addition, the recent activity of Standardization of concrete composite for radiation shielding in working group in AESJ would be introduced.